The Pennsylvania State University
The Graduate School

THE IMPACT OF PHOSPHOLIPID BILAYER INTERACTIONS ON LIPID DIFFUISON

A Dissertation in
Chemistry
by
Codey Henderson

Submitted in Partial Fulfillment
of the Requirements
for the Degree of

Doctor of Philosophy

December 2019

The dissertation of Codey Henderson was reviewed and approved* by the following:

Paul S. Cremer
J. Lloyd Huck Chair in Natural Sciences
Dissertation Advisor, Chair of Committee

Philip C. Bevilacqua
Distinguished Professor of Chemistry, Biochemistry, and Molecular Biology
Head of the Department of Chemistry

John B. Asbury
Associate Professor of Chemistry

Edward P. O'Brien
Associate Professor of Chemistry

Ester Gomez
Assistant Professor of Chemical Engineering

*Signatures are on file in the Graduate School.

Abstract

Herein, the diffusion of lipids in a supported lipid membrane is explored. Models for membrane lipid diffusion are first explored in context with modern experiments. A new model is proposed to reconcile differences between experimental results and model predictions revealing lipid diffusion's dependence on interactions between the substrate and the bilayer. Modulation of lipid diffusion is then accomplished by varying the substrate material, the bilayer composition, and the solution conditions. These modulations reveal more about the nature of the interactions and the forces at play. Additionally, evidence is provided for aggregation of lipid-conjugated dye within the bilayer, a necessary component for visualization under fluorescent microscopy. The results not only show direct visualization of the aggregates but also provide a molecular explanation for the fitting method utilized for fluorescence recovery after photobleaching experiments. Finally, this work extends the principles of lipid diffusion and fluorescence microscopy to synthetic water filtration membranes. Experimental support is provided for water transport mechanisms. This dissertation provides critical insights into how lipids interact with surroundings while anchored within a membrane and explores the critical factors affecting such interactions. The results herein can be applied not only to synthetic systems, but also to the cell to better understand the role of membrane interactions with cellular components.

Table of Contents

List of Figures

List of Symbols

F_t	Normalized fluorescence at a given time, p. 4
F_0	Normalized fluorescence at $t = 0$, p. 4
F_o	Normalized fluorescence prior to bleaching, p. 4
F_t	Normalized fluorescence at a given time, p. 4
a	Maximum normalized intensity recovered, mobile fraction, for a single exponential fit. Population weight for a double exponential fit, p. 4, 57
b	Exponential fitting term related to the time of half recovery, p. 4, 57
c	Population weight for a double exponential fit, p. 57
d	Exponential fitting term related to the time of half recovery, p. 57
$\tau_{1/2}$	Normalized fluorescence at a given time, p. 5
D	Translational diffusion coefficient, p. 5
w	Bleaching beam radius, p. 5
γ	Fitting term describing bleaching beam profile, p. 5
D_{SD}	Translational diffusion coefficient from the Saffman-Delbrück model, p. 18
k_B	Boltzmann constant, p. 18, 19, 20
T	Temperature, p. 18, 19, 20
μ_m	Membrane viscosity, p. 18
μ_f	Fluid viscosity, p. 18

h	Membrane height, p. 18
a_r	Radius of diffusing object, p. 18, 20
γ_E	Euler-Mascheroni constant, p. 18
D_{FV}	Translation diffusion coefficient from the extended free volume model, p. 19
γ_{FV}	Overlap of free area between two lipids, p. 19
T_m	Phase transition temperature, p. 19
a^*	Critical free area surrounding a lipid which will allow trnslocation, p. 19
a_o	Van der Waals area of the lipid, p. 19
$a_o\beta$	Free area at the phase transition temperature, p. 19
α_a	Lateral thermal expansion coefficient, p. 19
f	Translational friction coefficient, p. 19
f_w	Friction coefficient from surrounding water, p. 19
f_m	Friction coefficient from bilayer midplane, p. 19
f_s	Friction coefficient from the bilayer interacting with the surface, p. 20
η_w	Viscosity of bulk water, p. 20

Acknowledgments

I would like to acknowledge those who have helped me, both emotionally and educationally throughout this work. First, I would like to thank my advisor, Dr. Paul Cremer. I could listen to him talk about science for hours. His passion and drive to understand systems seeps deep into his work and it allows him to bring the work to life.

The lab manager, Tinglu, deserves a special thank you as well. His intricate knowledge about the instruments and the science they forward was invaluable to me. I am convinced there is no instrument he could not fix, operate, and interpret results from. Plus, he was an absolute joy to work with and never short of a smile. I truly appreciate all he has done for me and all he has taught me.

Many lab mates have helped me on my journey, and I would first like to thank my mentor and friend, Anne Sendecki. Her guidance and honesty helped me keep focus and understand the work. I would also like to thank other lab members, particularly Virginia Greenberger, Pho Bui, and Bradley Rogers for not only being excellent lab mates and friends, but also for their help and suggestions in compiling this dissertation. I could not have done it without them. I would also like to thank Chad Drexler for his friendly interactions and his enjoyment of talking about the science. Additionally, I would like to thank the previous lab members Simou Sun, Saranya Pullanchery, and Alexis Baxter for their kindness, input throughout my work, and great example of a scientist.

My family also deserves a special thank you for their love and support. Even though he is not a scientists, my dad has always sought to understand my work, to ask driving questions, and to motivate me to accomplish my goals. My whole family has always tried to talk to me about my research, forcing me to rethink how I describe it and helping me gain a better understanding through teaching.

My lovely wife, Kathleen, probably deserves the most gratitude for putting up with me. She has been an amazing support, encouraging me when things were rough and thrilled for me when I found success. This dissertation would have been truly impossible without her.

I would also like to thank my son, Sherwood. Thanks to him, I have not only learned about lipid bilayers, I have also learned the names and behaviors of more dinosaurs than Michael Crichton. His love for learning and desire to always know "why" is a constant encouragement for me to do better and reminder of how much more there is to learn.

This material is based upon work supported by Office of Naval Research under Award N00014- 14-1-0792. Any opinions, findings, and conclusions or recommendations expressed in this publication are those of the author(s) and do not necessarily reflect the views of the Office of Naval Research.

Dedication

This dissertation is dedicated to my family. My parents, for always being there for me with love and support. My siblings, for providing me with needed distractions and stimulation. My wife, for always believing in me and expecting me to conquer mountains. My children, for filling my life with joy and driving me to provide them with a better life. Thank y'all.

Chapter 1

Introduction

1.1 Phospholipid Bilayers and Lipid Diffusion

Phospholipids are produced by cells and self assemble into two-dimensionally fluid bilayers[1]. These bilayers surround cellular organelles, the nucleus, and the cell itself, creating a semipermiable barrier to various molecules and controlling the flux of molecules across the membrane[2][3]. By maintaining particle gradients across the membrane, bilayers aid in cellular processes[4]. Additionally, the cellular lipid membrane contains many proteins and peptides involved in a variety of processes including transport, production, and signalling[5][6][7]. The function of some such proteins is linked to the lipids themselves, as they preferentially embed in certain lipid regions[8]. Interestingly, the ability of a protein or peptide to interact with or potentially embed itself into the membrane requires the bilayer be fluid[9]. Additionally some proteins exist preferentially in certain lipid environments, indicating a tied functionality between the lipid and the protein[10][11]. While much work has been done to understand the protein functions in the bilayer, the focus on the role of lipids in the bilayer has only more recently been explored. A goal of this

work is to better understand the bilayer lipids' properties in various environments.

One such environment mimicked hereing is the cell's cytoskeleton. The cell's cytoskeleton supports the lipid bilayer, helping to provide structure and support to the membrane and to aid in spacial separation in the cell[12]. In eukaryotic cells, the cytoskeleton is composed of microscopic actin tubules and filaments which form a non-static network of underlying support[13]. Herein, the cytoskeleton is mimicked by a protein-passivated substrate, utilizing denature bovine serum albumin (BSA) to mimic amino acid-based interactions[14]. The protein-passivated substrate is observed to severely decrease lipid diffusion due to strong interactions between the protein's amino acids and the bilayer lipids. The work suggests the cellular stability from the cytoskeleton is not only resultant from a resistance to deformation, but is also a resultant from hindered diffusion by the strong, numerous protein-bilayer interactions.

To model the complex cellular membrane herein, various lipids are used, shown structurally in Figure 1.1. The most prevalent cellular membrane lipid, the zwitterionic lipid 1-palmitoyl -2-oleoyl-glycero-3-phosphocholine (POPC) was used in all bilayers as the primary component[15]. To modulate a negative charge in the bilayer, the negatively charged lipid 1-palmitoyl-2-oleoyl-sn-glycero-3-phosphate (POPA) was used. POPA has a pKa of 8.0, making it primarily singly charged at pH 7.4, the experimental pH[16]. To modulate a positive charge in the bilayer, the positively charged lipid 1,2-di-oleoyl-3-trimethylammonium-propane (DOTAP) was used. As seen structurally, the DOTAP head group is terminated by a quaternary amine, creating the lipid's positive charge. As the experiments in this work focus on fluorescence experiments, a fluorescent dye-conjugated lipid was added to bilayers. The dye used in most bilayers herein was Texas Red 1,2-dihexadecanoyl-sn-glycero-3-phosphoethanolamine (TR-DHPE).

This dissertation makes extensive use of a supported lipid bilayer, consisting of a two-dimensionally mobile lipid plane separated from a solid support by a small constrained water region, shown in Figure 1.2. The work herein explores methods to modulate the diffusion of lipids in such a system, including exploring the impact of other substrates with varying composition and topology. We focus on commonly used substrates including annealed borosilicate glass, mica, and fused quartz. These surface have seen broad applications instrumentally, including as fluorescence microscopy and atomic force microscopy substrates, as well as substrates for the study of biological samples[17][18][19][20]. While much work has been done to study bilayer formation on different substrates, this work looks to expand the understanding of how bilayer diffusion is affected by substrate conditions after bilayer formation. To this extent, we expand the knowledge of the nature of bilayer-substrate interactions.

1.2 Measuring Lipid Diffusion

While various methods exist for measuring lipid diffusion in a membrane, this work focuses on the use of fluorescence recovery after photobleaching (FRAP). In a FRAP experiment, a small amount of fluorescently labeled lipids are added to the bilayer. These lipids provide a means to visualize the bilayer under a fluorescent microscope; additionally, these fluorescent lipids act as a diffusion marker, providing a target whose movement can be monitored. The amount of fluorescent lipid is small enough so as to not expect a change in the membrane properties[21]. The amount is enough, however, to create a uniform sheet of fluorescent intensity when observed under a microscope, occurring for most dyes between 0.1 and 2 mol%[22][23]. The FRAP process is shown through a sample recovery curve in

Figure 1.3.

First, a laser is directed at the bilayer, causing photo-oxidation of the lipid-conjugated dye[24]. This bleaching event causes a dark region where the laser was targeted as approximately 10 to 15% of the dye molecules are no longer fluorescent[25][26]. Because the lipids have two dimensional mobility, the dark region will appear to defocus as bleached dye molecules randomly diffuse out of the bleached region and non-bleached dye molecules randomly diffuse in. Eventually, the dye molecules will be dispersed sufficiently such that the bilayer fluorescence appears uniform like prior to bleaching. The fluorescent intensity of the bleached region is therefore monitored over time to generate Figure 1.3.

The apparent defocusing of the bleached region is a result of the movement of the lipid-conjugated fluorescent dye. To this end the bleached region intensity is normalized to an unbleached region of the bilayer and the percent recovery at a given time is calculated according to the following equation,

$$F(t) = \frac{F_t - F_0}{F_o - F_0} \tag{1.1}$$

wherein F_t is the normalized fluorescence at a given time, t, F_0 is the normalized fluorescence intensity immediately following bleaching at t=0 seconds, and F_o is the normalized fluorescence intensity prior to bleaching[27]. The percent fluorescence recovery as a function of time can plotted and fitted to an exponential rise to max, as shown in the equation,

$$F(t) = a(1 - e^{-bt}) \tag{1.2}$$

wherein t is the time following bleaching, and a is the maximum normalized inten-

sity. This maximum is taken to represent the fraction of the bilayer able to freely diffuse, or the mobile fraction. The final term, b, is related to the time needed to reach half recovery. After using b to find the half recovery time, the time of half recovery is used to calculate a diffusion coefficient as follows,

$$\tau_{1/2} = \frac{ln(2)}{b} \tag{1.3}$$

$$D = \frac{w \cdot \gamma}{4\tau_{1/2}} \tag{1.4}$$

wherein $\tau_{1/2}$ is the time of half recovery, D is the diffusional coefficient, w describes the width of the laser beam, and γ is a correctional term descriptive of the laser beam shape and intensity distribution[25]. More precise variations of this approach have been suggested and used[27]. However, this method has been shown generally applicable and robust for a variety of lipid systems[28][29].

1.3 Lipid Membrane Models

Models are an important tool for understanding biological systems. Biological systems, especially cell membranes are extremely complicated with huge variety on the number and types of proteins, peptides, and even lipids present. A model can simplify the system by connecting system conditions to resultant effects. An effective should be applicable to as many of the conditions as possible while still retaining the simplicity to make it easily applied. Additionally, the model predictions and trends must be very well reconciled to experimental results. As better models are developed, they provide insights into the system and increase the ability

to predict cellular behaviors and understand mechanisms.

Multiple models have been developed to describe the phospholipid bilayer, the most famous of which is the fluid mosaic model. The fluid mosaic model is a qualitative description of the cellular membrane and describes proteins and other membrane bound components embedded within a lipid matrix[30]. The work herein focuses on the diffusion of the lipids themselves, and mathematical models have also been developed to describe lipid membrane diffusion. An early description of diffusion came through the Einstein-Stokes relation[31]. This description is general for any particle, including lipids, moving through a liquid and only captured some details of the particles themselves[32]. The model was developed further by Saffman and Delbrück, who described a membrane component as a simple cylinder diffusing in two dimensions through a viscous fluid[33]. In the model, a less viscous fluid above and below create a drag on the cylinder's ends. This model was an important step forward in understanding how objects interact with and move within the bilayer and still provides a reasonable estimation for transmembrane protein diffusion[34]. However, the model has limitations for small diameter particles, particularly lipids. To this end, a model was proposed by Thompson et al.[35], which built upon the free volume model of Turnbull and Cohen[36]. This extended free volume model corrected the previous models' temperature dependence by utilizing the volume required for lipids to slip by one another. Unfortunately, the bilayers used in this model were a multilamellar mixture of structures rather than the unilamellar supported bilayers used in the more recently developed supported lipid membrane platforms[37]. As a result, the model is more fitting to a non-supported or partially supported bilayer, consistent with its inception as an extension of the free volume model for phase transition[36]. This dissertation explores experimental data from unilamellar supported lipid membranes and further modifies the

extended free volume model to account for substrate interactions. As such, this work furthers the existing membrane models to better describe and understand the supported lipid membrane.

1.4 Dye Aggregation

The fitting of FRAP data by a single exponential rise to maximum suggests the lipids in a supported membrane can be described as a single type of molecule and all the lipids are in the same average environment. The degree to which this is true varies depending on the membrane, but for a simple model membrane this assumption is generally accepted[28]. However, work done herein at very low lipid-conjugated dye concentration suggest even in very simple bilayers this assumption is not true. The dye used to visualize the bilayer has been shown to create aggregates, likely even involving the non-fluorescent bilayer lipids. These aggregates vary in size, creating a distribution of lipid environments and therefore a distribution of diffusion rates. Herein, we connect this distribution to the fitting of a FRAP curve. We further suggest the need to fit to a double exponential to better describe the multiple lipid conditions.

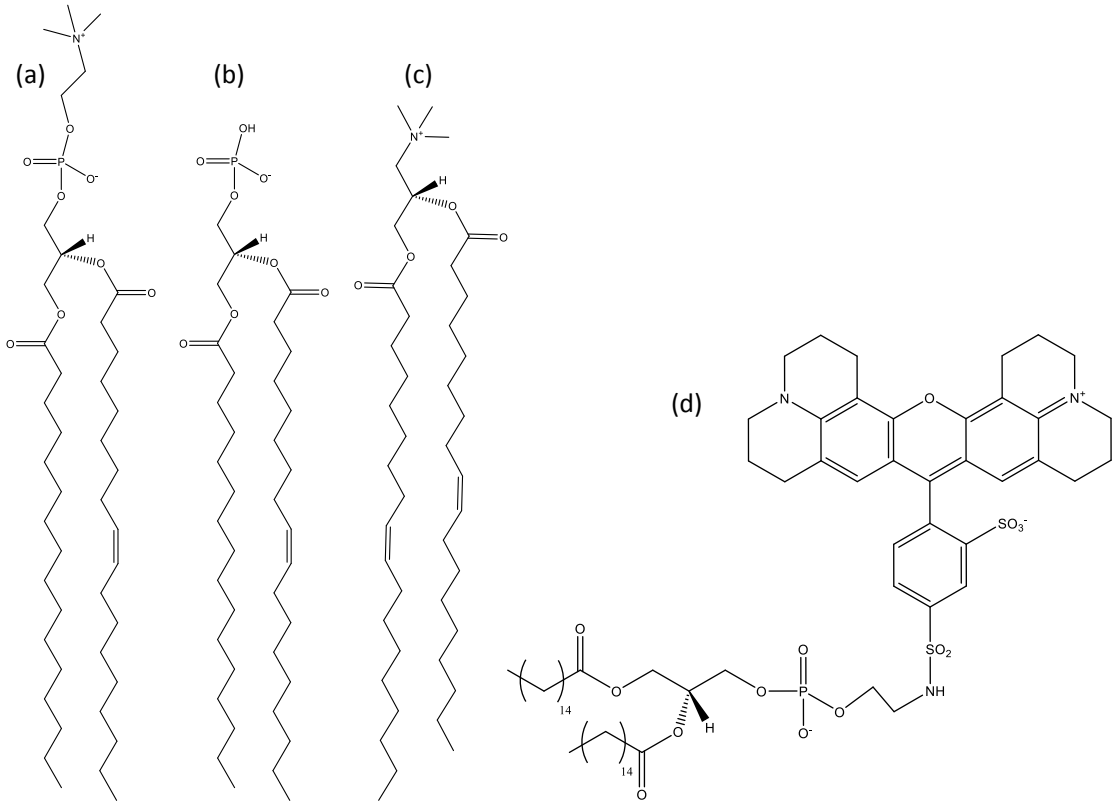

Figure 1.1. Strucutre of Phospholipids. Shown are the structures for (a) POPC, (b) POPA, (c) DOTAP, and (d) TR-DHPE

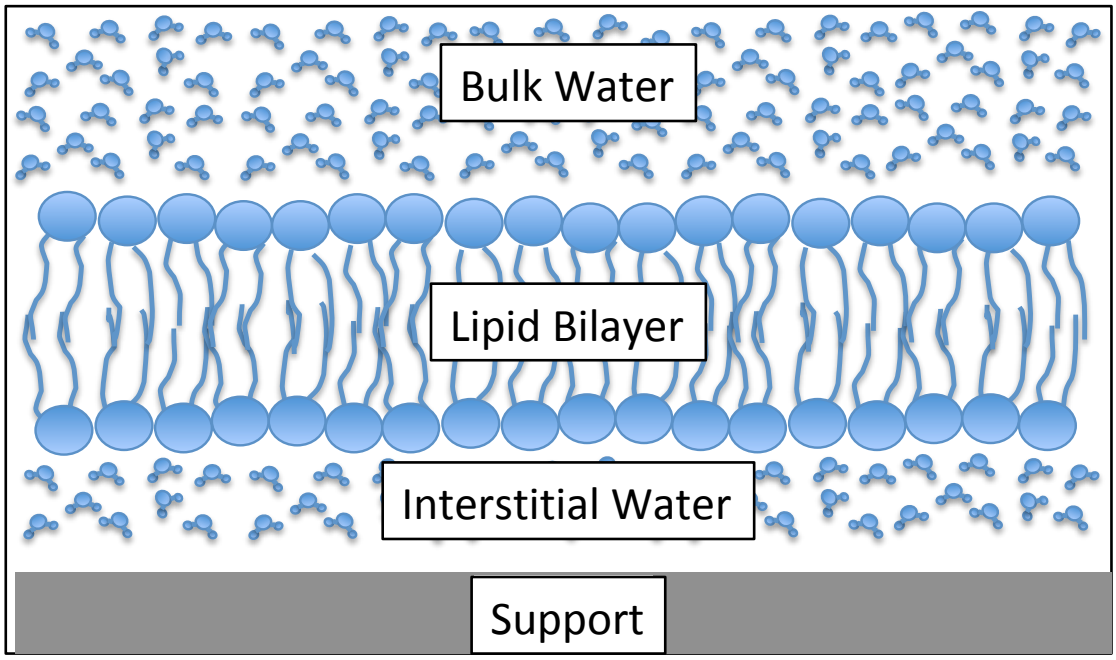

Figure 1.2. Schematic of a Supported Lipid Bilayer. A typical support used experimentally is glass. Shown also is the interstitial water layer, formed between the support and lipid bilayer.

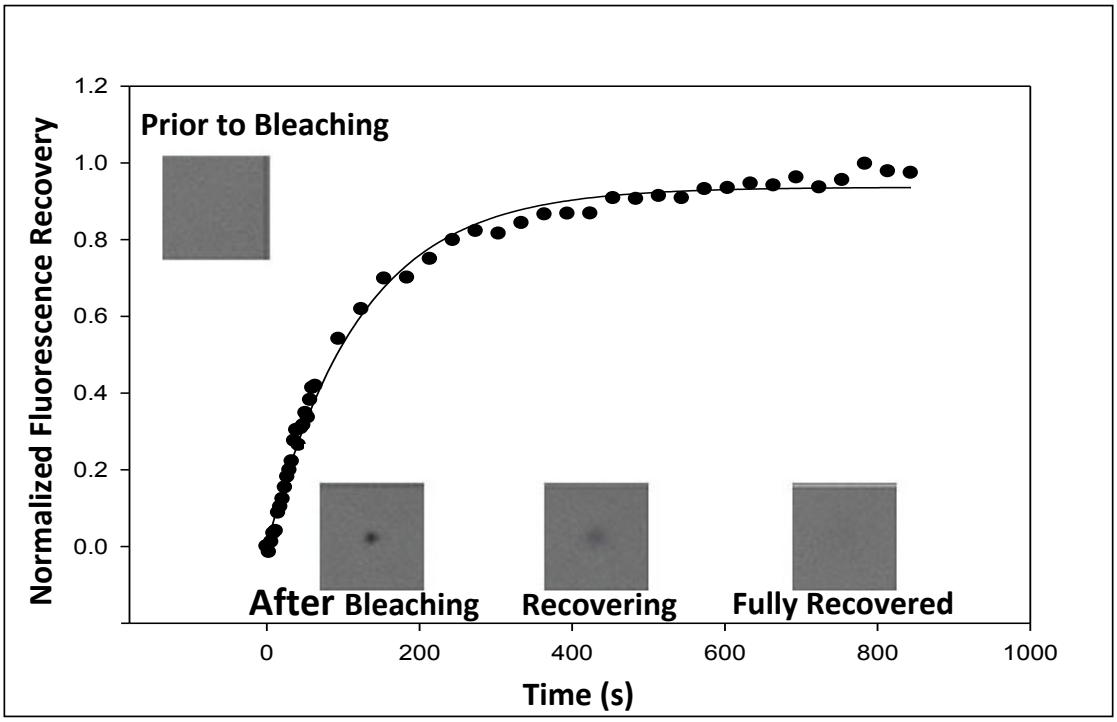

Figure 1.3. Sample Fluorescence Recovery After Photobleaching Curve. Sample bilayer consists of 99.5 mol% POPC and 0.5 mol% TR-DHPE supported by annealed borosilicate glass. Prior to bleaching, bilayer fluorescence is uniform and even. Immediately following laser exposure, a dark region is observed wherein 10 to 15 % of the fluorescent dye has been bleached. The bilayer is then observed to recover, as the lipids within the bilayer diffuse randomly in and out of the bleached area. After some time, the bilayer intensity fully recovers to pre-bleach intensity.

Chapter 2

Modeling the Effect of Temperature on Supported Lipid Bilayer Diffusion

2.1 Introduction

Cellular membranes are formed by phospholipid bilayers and act as a semipermeable barrier, controlling the flow of material in and out of the cell[38]. Proteins and other membrane-associated materials serve many cellular functions, including transport and signaling[39]. The cytoskeleton and extracellular support reinforce the bilayer and help to maintain its form[40]. The bilayer is not, however, static; lipids move two-dimensionally within the bilayer and can flip from the top leaflet to the bottom leaflet and vice-versa with the aid of specialized proteins[41]. Some functions, such as cooperative binding to the bilayer, would be impossible without fluidity of the bilayer[42][43]. Many features, specifically bilayer composition and interactions with a support, impact fluidity of the bilayer. The most notable impact of bilayer composition is the melting temperature of the lipids. Depending on the lipids, the bilayer may be in a gel or liquid phase at room temperature. For

example, 1-palmitoyl-2-oleoyl-sn-glycero-3-phosphocholine (POPC) has one degree of unsaturation in the tail region and has a melting temperature of -2 °C and is therefore in the liquid phase as room temperature[44]. Likewise, 1,2-dipalmitoyl-sn-glycero-3-phosphocholine (DPPC) has the same head group but with fully saturated tails and as a result, a melting temperature of 41 °C; DPPC is therefore in a gel phase at room temperature[45]. A bilayer in the gel phase, such as DPPC at room temperature, diffuses very slowly and is often considered immobile. A bilayer in the liquid phase, however, diffuses noticeably in the presence or absence of a support[46].

The study of bilayer physical properties, including the above discussed phase transitions, is often done in model phospholipid membrane systems. Two of the most common biomimetic methods to study bilayer properties are Giant Unilamellar Vesicles (GUVs) and Supported Lipid Bilayers (SLBs). In a GUV, two frictional forces hinder lipid movement within the bilayer, namely the drag from one leaflet tail to the other and the drag from the lipid head interacting with the water. In an SLB, the bilayer sits 1 nm above a solid support with a thin layer of water between the support and bottom leaflet[47].

Interactions of the bilayer with the support and water layer, be it electrostatics, van der Waals, or hydrogen bonding, cause a decrease in the fluidity and therefore a decrease in the diffusion of the bilayer. As a result, the bilayer diffuses approximately five times slower for an SLB than for a GUV[48]. One may think the movement of only the leaflet adjacent to the substrate would be significantly retarded, however the tail interactions are strong such that only approximately 5% difference in the diffusion is observed between the top, distal leaflet and bottom, proximal leaflet[49]. This difference in diffusion is insignificant and within error of the measurements used herein. As such, the leaflets will be considered to move

together unless otherwise noted.

Fluidity can be measured by multiple techniques, namely nuclear magnetic resonance, electron spin resonance, and fluorescence techniques[50]. Unfortunately, most techniques require probes and sample preparation prior to experimentation. For example, this experiment uses a lipid labeled with a fluorescent group, Texas Red. The mobility of the bilayer is inferred based on the mobility of Texas Red. The mobility of the dye is tied to the bilayer mobility though the value obtained may differ for each dye; as such, care must be taken when comparing diffusion coefficients from one dye to another.

The most commonly used method to measure fluidity and the method employed herein is FRAP[51]. As discussed in Chapter 1 of this dissertation, FRAP consists of focusing a laser on a fluorescent bilayer; a percentage of the fluorophores in the region are irreversibly photobleached, resulting in an observed dark spot. Over time, the bleached and unbleached fluorophores diffuse randomly two-dimensionally within the bilayer, causing the dark spot to appear to spread and fade. After roughly 10 minutes (depending on the sample) the bleached area appears like the bilayer prior to bleaching as the photobleached molecules are now dispersed throughout the bilayer[25].

To help understand the supported membrane system and the nature of the bilayer properties, mathematical models are employed. Models help provide proof of concept for explanations to observed phenomena[52]. In the case of bilayer diffusion, these phenomena include the underlying interactions present as well as the response to certain stimuli. The most basic description of diffusion stems to the Einstein-Stokes relationship correlating the diffusion rate of any particle to the temperature of the system, the viscosity of the medium, and the size of the particle[31]. While simplistic in nature, the model provides a surprisingly applica-

ble and modifiable basis to describe diffusion[53][54][55]. Herein, FRAP is used to investigate the effect of temperature on supported phospholipid bilayer diffusion. Experimental data are compared to expectations from the Saffman-Delbrück and extended free volume mathematical models. The extended free volume model is modified and reconciled to the data, providing a new model for lipid diffusion in a supported membrane. Although the difference in SLB and GUV lipid diffusion has previously shown the effect of a substrate on lipid diffusion, the new model provides proof of the substrate coupling with the bilayer and inducing changes in lipid diffusion.

2.2 Materials and Methods

2.2.1 Materials

Borosilicate glass microscope slides were obtained from Fisher Scientific (Hampton, NH). Sodium chloride salt was purchased from DOT Scientific Inc. (Burton, MI). Tris(hydroxymethyl)aminomethane salt (Tris) was purchased from Calbiochem (San Diego, CA). Polydimethylsiloxane (PDMS) was obtained from Dow Corning (Midland, MI) as Sylgard, silicone elastomer-184.

POPC was purchased in chloroform from Avanti Polar Lipids, Inc. (Alabaster, AL). TR-DHPE was obtained from Life Technologies (Grand Island, NY).

A temperature-programmable circulator was obtained from VWR International (Radnor, PA). Lipid extrusion was performed with a 10 mL LIPEX Extruder purchased from Northern Lipids Inc (Vancouver, Canada) using 200 nm Whatman track-etch membrane filters (Maidstone, United Kingdom).

2.2.2 Methods

Fluorescence Recovery After Photobleaching

FRAP was performed on a home-built instrument including a Nikon Eclipse TE2000-U microscope with an X-Cite Series 120 halogen light source. Bleaching of the TR-DHPE lipid was accomplished with an Opto Engine LLC MGL-III-532 300 mW 532 nm laser with a PSU-III-FDA power source. Laser power was reduced in the optical train to approximately 5 mW at the microscope stage. The sample was exposed to the laser for approximately 2 seconds for the initial bleaching event. The laser beam was fit to a Gaussian and the radius was found as the full width at half maximum. The intensity of the bleached region was measure prior to and after bleaching and corrected to a similar, unbleached region of the bilayer. The region intensity was monitored until full recovery observed, as evident by the leveling off of the region intensity. The bleached region intensity was normalized to an unbleached region of the bilayer and the percent recovery at a given time was calculated according to Equation 1.1. The percent fluorescence recovery as a function of time was plotted and fit to an exponential rise to maximum according to Equation 1.2 to extract the mobile fraction and the $\tau_{1/2}$ from Equation 1.3. The time of half recovery was then used to calculate the translational diffusion coefficient of the bilayer from Equaiton 1.4. The correctional term, γ, was taken to be 0.88 for the TE2000-U microscope configuration.

Substrate Preparation

Borosilicate float glass cover slips were first cleaned in a 1:7 diluted solution of 7X detergent and 18.2 MΩ deionized water for 1.5 hours at 80 °C. Slides were then rinsed with copious amounts of 18.2 MΩ water, soaked in 18.2 MΩ water for 1.5 hours at 80 °C, and dried under a stream of nitrogen until not water was visible,

approximately 5 minutes. Substrate samples were further treated by annealing at 550 °C for 6 hours[56].

Lipid Vesicle Formation

Lipid vesicles were prepared by the freeze thaw extrusion method. Various amounts of POPC and TR-DHPE corresponding to the desired mole ratio were mixed in chloroform, and then dried under nitrogen. The dried lipids were placed under vacuum for at least two hours to remove any residual chloroform. The lipid films were then rehydrated in buffer solution (100 mM NaCl, 10 mM Tris) at pH 7.4 to a concentration of 1 mg/mL. The vial containing lipid solution was sonicated for 10 minutes to ensure complete rehydration of the lipids. The lipids spontaneously form multilamellar vesicles of varying size upon rehydration. The lipid solution was then put through 10 freeze thaw cycles by alternating liquid nitrogen and warm water (approximately 70 °C). The lipids were then extruded through a polycarbonate membrane with 200 nm pores[57]. The freeze thaw cycles and extrusion create unilammelar vesicles of consistent size. Vesicle size was confirmed by dynamic light scattering and the average vesicle size was approximately 130 nm.

Lipid Bilayer Formation

A PDMS well was placed atop the prepared borosilicate slide and 75 μL vesicle solution was added into the well. The vesicles were allowed 20 min for fusion to spontaneously occur. Excess lipids were then rinsed off with 18.2 MΩ water. To create contrast for fluorescent imaging, a scratch was made to the bilayer by gently running tweezers along the substrate after bilayer fusion. The bilayer was subsequently rinsed with excess 18.2 MΩ water. For bilayers formed at elevated temperature, the substrate and PDMS well were preheated and the temperature

was maintained as the vesicle fusion occurred. Additionally for the bilayers formed at elevated temperature, the sample was rinsed with warm 18.2 MΩ water prior to and after the scratch was made. For samples heated throughout the experiment or maintained at an elevated temperature, the PDMS well with the now formed lipid bilayer was then sealed by capping the well with a cleaned glass cover slide. Additional experiments were done wherein all rinsing steps were instead performed with buffer containing 100 mM NaCl and 10 mM Tris at pH 7.4; however, no difference was observed in experimental results.

Temperature Control

A hollow aluminum block with a circular hole in the center was connected to the temperature-programmable circulator. The aluminum block was placed on top of the sample, with the PDMS well inside the aluminum block's hole. Additionally, the hole in the aluminum block was covered to reduce temperature fluctuation. A thermocouple was used to monitor the bilayer temperature by measuring the substrate temperature on the side opposite to the bilayer. When the temperature was changed, a minimum of 30 minutes was allowed for re-equilibration at the new temperature.

2.3 Results and Discussion

Fluidity of the bilayer has been described through multiple models; the most widely used model is the Saffman-Delbrück model[33]. The model describes the Brownian diffusion of a cylindrical object within a viscous, three-dimensional plane of thickness equal to the cylinder. Above and below the plane is a much less viscous fluid. Both the plane itself and the surrounding fluid are assumed to have no specific interactions with the embedded object. Applied to a lipid bilayer, the

model predicts a temperature dependence of the diffusion coefficient, shown below in Equation 2.1,

$$D_{SD} = \frac{k_B T}{4\pi\mu_m h} \cdot [ln(\frac{\mu_m h}{\mu_f a_r}) - \gamma_E] \tag{2.1}$$

in which k_B is the Boltzmann constant, T is the system temperature, μ_m is the membrane viscosity, h is the membrane height, μ_f is the viscosity of the surrounding fluid, water, a_r is the radius of the object diffusing, and γ_E is the Euler-Mascheroni constant, 0.577. To predict the impact of temperature on the diffusion, a ratio of the TR-DHPE lipid's diffusion coefficient in a POPC bilayer at high temperature versus low temperature ($\frac{D_H}{D_L}$) was analyzed. After an approximation for the bilayer viscosity, the diffusion coefficient at 50 °C, D_H, was calculated as 2.2 $\mu m^2 s^{-1}$, approximately 1.5 times greater than the diffusion coefficient at 23 °C, $D_L = 1.5\ \mu m^2 s^{-1}$, shown as the blue inverted triangles in Figure 2.1.

Surprisingly, the Saffman-Delbrück model prediction is much lower than what has now been observed for a typical supported lipid bilayer, for which D_H was approximately 4 times higher than D_L for the same temperature range, shown as black squares in Figure 2.1. The work herein suggests the model fails because no term in the equation accounts for the difference in fluidity of the top, distal water and the bottom, proximal water or for the possibility of bilayer-substrate interactions. Additionally, the extended free volume model claims the Saffman-Delbrück model fails because the lipid of interest is too small for the surrounding lipids to be considered a continuous fluid[35].

To explore the possibility the phenomenon is dependent on bilayer formation and defects, obtained diffusion coefficients at various temperatures were compared for lipid bilayers formed at 23 °C to lipid bilayers formed at 37 °C. Interestingly, the

diffusion of the bilayer and mobile fraction was found independent of the formation temperature. As the formation temperature impacts the completion and presence of defects in the lipid bilayer, the results imply the defect differences in lipid bilayers formed 23 °C and 37 °C are not responsible for the observed temperature dependence.

Work has been done to extend the free volume model to lipid systems and manages to predict a larger change in diffusion with temperature than the Saffman-Delbrück model[35]. The model utilizes a free volume required for one lipid to slip past another lipid and takes the form of Equation 2.2,

$$D_{FV} = \frac{k_B T}{f} \cdot exp[\frac{-\gamma_{FV} a^*}{a_o(\beta + \alpha_a(T - T_m))}] \tag{2.2}$$

in which T_m is the phase transition temperature of the lipids in the membrane, γ_{FV} is the overlap of free area between two lipids, a^* is the critical free area surrounding a molecule which will allow translocation, a_o is the van der Waals area of the lipid, $a_o\beta$ is the free area at T_m, and α_a is the lateral thermal expansion coefficient in the liquid crystalline phase. The term f is the translational friction coefficient and is considered in Vaz et al. to be $f = f_w + f_m$[35], or the sum of the friction coefficients from the drag forces of the surrounding water (f_w) and of the bilayer midplane (f_m). Using the approximations given by Vaz et al.[35], the green triangle points in Figure 2.1 were obtained.

Although the extended free volume model gives a closer approximation than the Saffman-Delbrück model, the extended free volume model predicted values still fall short of the large temperature dependence of the experimentally obtained data. To this end another frictional coefficient term was added to account for the

association of the bilayer with the surface, f_s. Values for f_s were determined as

$$f_s = \frac{1}{1 + e^{(k_B T)/x}} \tag{2.3}$$

in which x was first solved to fit the experimental data at 23 °C and had a value of 2.7×10^{-22}. It should be noted the frictional term, f_s, simply suggests a high viscosity, restrained region between the bilayer and the substrate; no atomic indication is made as to the source of the restraint, be it from highly constrained hydrogen bonded water, salt bridging, or direct interactions between the substrate and lipid bilayer. Furthermore, the equation for f_s is not based upon specific physical principles, but is rather purely phenomenological. Further work will need to be done to derive an equation which is based on statistical mechanical arguments.

f_s was then solved for across the experimental temperature range and had the values shown in Figure 2.2.The values for f_s show a decrease as temperature increases, as expected. As the temperature increases, the interactions between the bilayer and the substrate should break and result in a decrease of the overall adhesion of the bilayer to the substrate, as reflected in a smaller value of f_s.

Values from the extended free volume model were unaltered from Vaz et al.s approximation[35]. f_w was approximated by the Stokes relation, $f_w = 6\pi\eta_w a_r$, utilizing the viscosity of bulk water, η_w; this viscosity was adjusted by fitting the calculated diffusion coefficient to the experimental diffusion coefficient at 23 °C. The value of η_w was then assumed to vary with temperature in accordance to the change in bulk water viscosity. It should be noted the water around the lipid heads should be considerably more restricted than bulk water, a factor accounted for by fitting to the experimental diffusion coefficient at 23 °C. The breaking of the water constraint near the lipid head groups is unlikely to be the same as breaking

bulk water structure and therefore the change in water viscosity with temperature would not be the same. Additionally, f_m was assumed to be invariable across the experimental range. For a fluid bilayer well above the melting phase transition, this assumption is accurate for this temperature range. The addition of the third frictional term results in a very good fit to the data, shown as the red circles in Figure 2.1.

The interaction between the surface and the bilayer was further examined by plotting $ln(f_s)$ versus $1/T$, as shown in Figure 2.3. According to the Arrhenius equation, the linear fit of this plot should have a slope equal to $-E_a/R$, wherein E_a is the activation energy of the process. By the fit, the activation energy to overcome this barrier is 38 kJ/mol, roughly the energy to break 2 liquid water hydrogen bonds[58]. This value is consistent with the bilayer coupled to the substrate through a constrained water region.

The close fitting with a small change to the total friction exerted on the diffusing lipid shows the consistencies within the free volume concept. By the model, the movement of a lipid is dependent on the creation of a volume around the lipid wherein the lipid is able to slip by another lipid. The parameters for this volume remains unchanged in the modified model and confirms the lipids are behaving as expected, with dependence on the free area of the lipids, the overlap of area, and the bilayer thermal expansion. The modified model instead simply suggests the method for calculating the lipid coupling to its environment is incorrect for a supported system. Instead, the coupling to the substrate must also be accounted for. The new model also suggests how the temperature affects this bilayer-substrate coupling and provides an effective means to estimate lipid diffusion in a supported lipid bilayer. Furthermore, the new model highlights the important role of bilayer-substrate coupling in the diffusion of lipids.

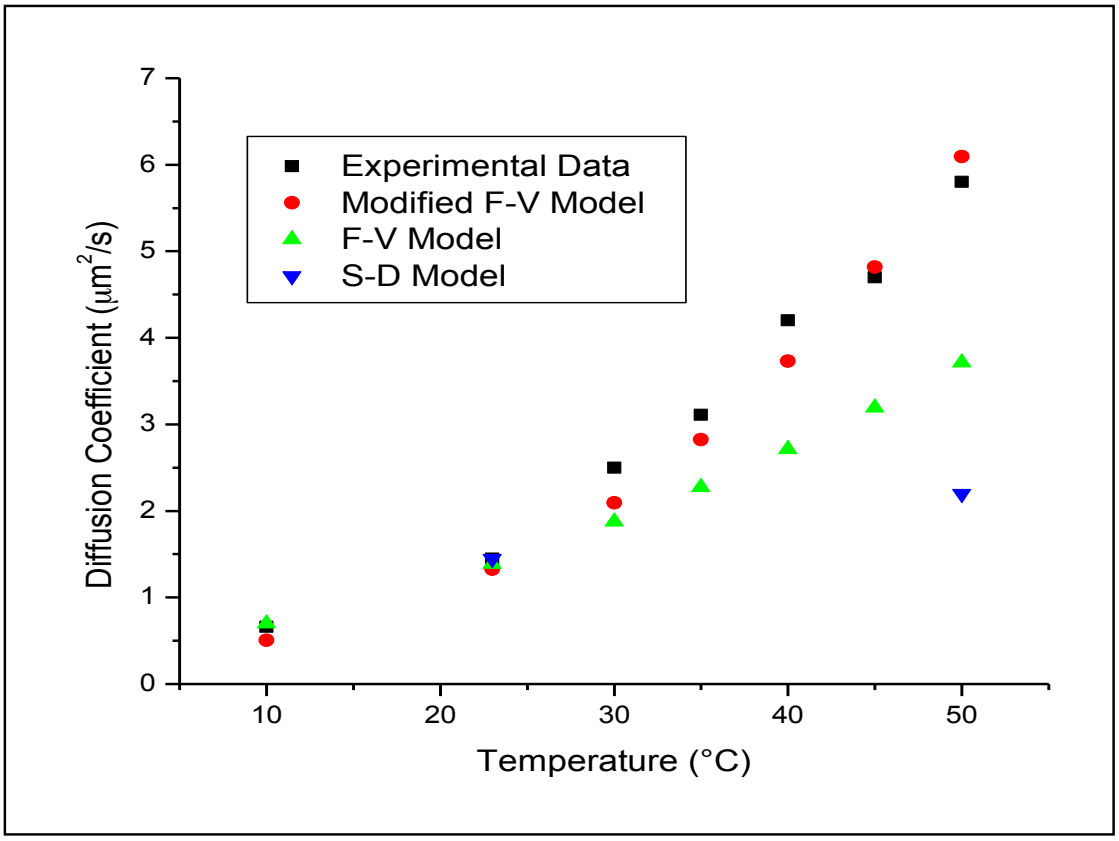

Figure 2.1. Typical Diffusion at Various Temperatures and the Predictions of Various Models. Shown is the collected data of bilayer diffusion on annealed borosilicate (black square), Saffman-Delbrück model predictions (blue inverted triangle), extended free volume model (green triangle), and the extended free-volume model modified to include bilayer-substrate friction (red circle).

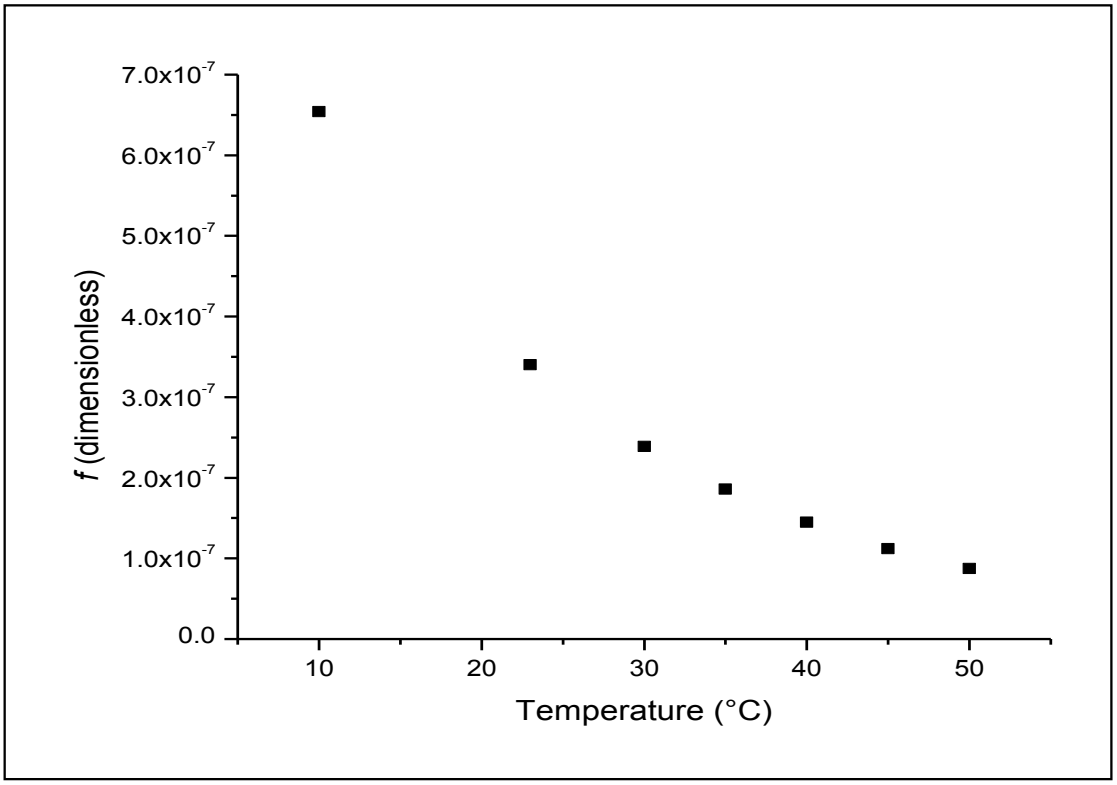

Figure 2.2. Calculated Values for f at Various Temperatures. Shown are values for the substrate-bilayer frictional coefficient, f_s (black square) calculated for a 99.5/0.5 mol% POPC/TR-DHPE bilayer formed on annealed borosilicate.

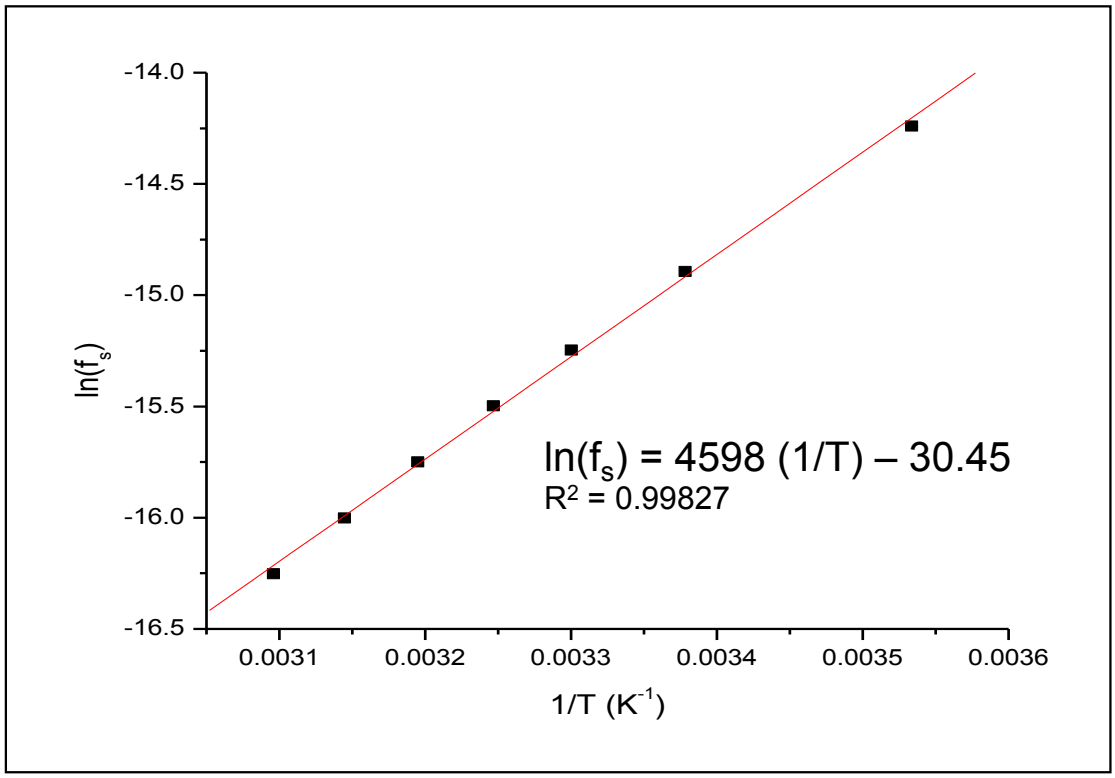

Figure 2.3. Arrhenius Plot of f_s. Shown is the linear fit for an Arrhenius plot of f_s for a 99.5/0.5 mol% POPC/TR-DHPE bilayer formed on annealed borosilicate.

Chapter 3

Modulation of the Bilayer-Substrate Interactions

3.1 Introduction

Phospholipid membranes form a semipermiable protective barrier around cells to help control cellular functions and conditions[59][60]. These lipid membranes are extremely complicated, with different membrane components present in different amounts depending on the cellular conditions and biological purposes[61][62]. As cellular function is extremely complex and therefore difficult to study, biomimetic model systems are often employed to focus a study on specific properties[63]. Two common biomimetic systems are GUVs and SLBs. GUVs are free-floating spherical bilayers, which are commonly used to study the flow of material across the membrane[64][65]. SLBs are planar bilayers formed over a solid support with a sub-nanometer layer of water between the bilayer and the support. SLBs are useful for fluorescence experiments, especially for studying particle interactions with the bilayer, sensing assays, and phase separation of lipid rafts[66][67][68]. Unfor-

tunately, SLBs generally are not well suited for studying transmembrane protein functions, as the proximal leaflet (bilayer leaflet closest to the support) is close enough to the support such that the protein will denature as it comes in direct contact with the substrate; hence, work has been done to separate the bilayer from its underlying support[69][70].

An important attribute of lipid bilayers is fluidity as it allows for the function of membrane and membrane bound component, including proteins[71]. The lipids in a GUV are known to diffuse much more quickly than the lipids in an SLB[72]. The most pronounced difference between a GUV and SLB is the presence of a support; hence, the interactions between the substrate and lipid bilayer must be responsible for the decreased lipid fluidity in an SLB. Interestingly, the diffusion of lipids in an SLB is much closer to the lipid diffusion observed in actual cells[73][50]. A living cell has multiple factors contributing to the decreased diffusion, namely a viscous inner fluid, a supportive actin-based cytoskeleton, and the presence of many bilayer components such as proteins, cholesterol, and associated materials, many of which may be charged[74][75][76][77]. To explore the effects of these cellular components on diffusion, a model POPC supported lipid bilayer was employed. The impact of the substrate characteristics, the bilayer composition, and the solution conditions on bilayer fluidity was elucidated by employing fluorescence microscopy.

3.2 Materials and Methods

3.2.1 Materials

Borosilicate glass microscope slides were purchased from Fisher Scientific (Hampton, NH). Fused quartz slides were purchased from Quartz Plus Inc. (Brookline,

NH). Muscovite mica was purchased from Ted Pella Inc. (Redding, CA). Bovine serum albumin fluorescently labeled with Alexa Fluor 488 (BSA) was purchased from Life Technologies (Carlsbad, CA).

POPC, DOTAP, and POPA in chloroform as well as cholesterol powder were all obtained from Avanti Polar Lipids, Inc. (Alabaster, AL). TR-DHPE was obtained from Life Technologies (Grand Island, NY).

Sodium chloride salt was purchased from DOT Scientific Inc. (Burton, MI). Calcium chloride salt was purchased from Sigma-Aldrich (St. Louis, MO). Tris buffer salt was purchased from Calbiochem (San Diego, CA). PDMS was obtained from Dow Corning (Midland, MI) as Sylgard, silicone elastomer-184. For temperature control, a temperature-programmable circulator was obtained from VWR International (Radnor, PA).

Lipid extrusion was performed with a 10 mL LIPEX Extruder purchased from Northern Lipids Inc (Vancouver, Canada) using 200 nm Whatman track-etch membrane filters (Maidstone, United Kingdom).

3.2.2 Methods

Fluorescence Recovery After Photobleaching

Fluorescent experiments were carried out on a custom-built Nikon Eclipse Ti inverted fluorescent microscope equipped with a Hamamatsu C11440 CCD camera. Sample was illuminated with 561 nm light generated by an Aura II 4-NII-FA LED source. Sample bleaching was accomplished by a 561 nm laser generated by a Nikon LU-N3 laser box and directed by a Bruker Miniscanner. A 30 μm diameter circle was bleached by targeting each pixel for 30 μs with an approximately 5 mW 532 nm laser. The laser would scan through the pixels, returning to the first after all pixels

had been targeted, until a total time of 3 seconds was accomplished. Although this does allow for some diffusion while the bilayer is bleached, the diffusion in the bleached region is significantly slower than the bleaching time; additionally, a line scan of the bleached region intensity revealed the region was evenly bleached relative to the bilayer. The intensity of the bleached region was measure prior to and after bleaching and corrected to a similar, unbleached region of the bilayer. The spot intensity was monitored until full recovery observed, as evident by the leveling off of the spot intensity. The bleached region intensity was normalized to an unbleached region of the bilayer and the percent recovery at a given time was calculated according to Equation 1.1. The percent fluorescence recovery as a function of time was plotted and fit to an exponential rise to maximum, as shown in Equation 1.2. The maximum is taken to represent the fraction of the bilayer able to freely diffuse, or the mobile fraction. The fit is used to calculate $\tau_{1/2}$ from Equation 1.3. $t_{1/2}$ is then used to calculate the diffusion coefficient from Equation 1.4. The correctional term, γ, was taken to be 1.0 for cylindrical-bleaching Eclipse Ti microscope configuration.

Preparation of Annealed Borosilicate Float Glass

Borosilicate float glass cover slips were first cleaned in a 1:7 dilute solution of 7X detergent and 18.2 MΩ water for 1.5 hours at 80 °C. Slides were then rinsed with copious amounts of 18.2 MΩ water and soaked in 18.2 MΩ water for 1.5 hours at 80 C. The slides were then dried under a stream of nitrogen. Finally, samples were treated by annealing at 550 °C for 6 hours[56]. Annealed borosilicate was then ready for use.

Preparation of Non-Annealed Borosilicate Float Glass

Borosilicate float glass cover slips were first cleaned in a 1:7 dilute solution of

7X detergent and 18.2 MΩ water for 1.5 hours at 80 °C. Slides were then rinsed with copious amounts of 18.2 MΩ water and soaked in 18.2 MΩ water for 1.5 hours at 80 C. The slides were dried under a stream of nitrogen. Non-annealed samples were then ready for use.

Preparation of Fused Quartz

Fused quartz slides were first cleaned in a 1:7 solution of 7X detergent and 18.2 MΩ water for 1.5 hours at 80 °C. Slides were then rinsed with copious amounts of 18.2 MΩ water and soaked in 18.2 MΩ water for 1.5 hours at 80 °C. and dried under a stream of nitrogen. Quartz samples were further treated by heating at 550 °C for 6 hours. Note that 550 °C is well below the annealing temperature of quartz; therefore, this heating only removed potential contaminants and did not affect the surface topology.

Preparation of Mica

Immediately prior to use, mica was freshly cleaved to create a new, clean surface for use. No further treatment was necessary

Preparation of Protein Passivated Annealed Borosilicate Glass

A PDMS well was first placed on a fresh annealed borosilicate float glass slide. 50 μL of a 0.1 mg/mL solution of BSA in buffer containing 100 mM NaCl and 10 mM Tris at pH 7.4 was added to the well and allowed to incubate for 20 minutes. The surface was then rinsed with buffer. Vesicle solution was then mixed with the now present solution for bilayer formation.

Lipid Vesicle Formation

Lipid vesicles were prepared by the freeze thaw extrusion method. Various amounts of POPC, DOTAP, POPA, Cholesterol, and TR-DHPE corresponding to

the desired mole ratio were mixed in chloroform then dried under nitrogen. The dried lipids were placed under vacuum for at least two hours to remove any residual chloroform. The lipid films were then rehydrated in buffer solution (100 mM NaCl, 10 mM Tris) at pH 7.4 to a concentration of 1 mg/mL. The vial containing lipid solution was sonicated for 10 minutes to ensure rehydration of the lipids. The lipids spontaneously form multilamellar vesicles of varying size upon rehydration. The lipid solution was then put through 10 freeze thaw cycles by alternating the vial between liquid nitrogen and a hot water bath. The lipids were then extruded through a polycarbonate membrane with 200 nm pores[57]. The freeze thaw cycles and extrusion create unilammelar vesicles of consistent size. Vesicle size was confirmed by dynamic light scattering and the average vesicle size was approximately 130 nm.

Lipid Bilayer Formation

A PDMS well was placed atop the prepared substrate and 75 μL vesicle solution was added into the well. The vesicles were allowed 20 minutes for fusion to spontaneously occur. Excess lipids were then rinsed off with 18.2 MΩ water. To provide contrast for fluorescence microscopy, a scratch made to the bilayer by gently running tweezers along the substrate and the bilayer was subsequently rinsed with excess 18.2 MΩ water. For bilayers formed at elevated temperature, the substrate and PDMS well were preheated and the temperature was maintained as the vesicle fusion occurred. Additionally for the bilayers formed at elevated temperature, the sample was rinsed with warm 18.2 MΩ water prior to and after the scratch was made. For samples heated throughout the experiment or maintained at an elevated temperature, the PDMS well with the now formed lipid bilayer was then sealed by capping the well with a cleaned glass cover slide. Additional experiments

were done wherein all rinsing steps were instead performed with buffer containing 100 mM NaCl and 10 mM Tris at pH 7.4; however, no difference was observed in experimental results.

Temperature Control

A hollow aluminum block with a circular hole in the center was connected to a temperature-programmable circulator (VWR). The aluminum block was placed on top of the sample, with the PDMS well inside the aluminum block's hole. Additionally, the hole in the aluminum block was covered to reduce temperature fluctuation. A thermocouple was used to monitor the bilayer temeprature by measuring the substrate temperature on the side opposite to the bilayer. When the temperature was changed, a minimum of 30 minutes was allowed for re-equilibration at the new temperature.

3.3 Results and Discussion

3.3.1 Impact of Substrate Topology on Lipid Bilayer Diffusion

To explore the impact of the substrate on bilayer-substrate coupling, topographical and diffusion data were compared for substrates with different composition. Chemically, the borosilicate and quartz glasses are similar since both contain silicon dioxide as a primary component[78]. In addition to silicon dioxide, the borosilicate glass has additional ions, including boron, sodium, and aluminum. Unlike the borosilicate glass, the quartz glass is formed from very high purity silicon dioxide sand and is therefore assumed to contain few if any contaminants. Physically, the borosilicate and quartz surfaces have vast differences, as differences in the

preparation have created vastly different surface topologies, as seen in Figure 3.1. Annealed borosilicate was observed to have a consistently flat surface with a 0.48 nm rms roughness. In contrast, quartz was observed to have a highly inconsistent surface with a 9.26 nm rms roughness, almost 20 times higher than annealed borosilicate.

In the case of the annealed borosilicate, the annealing process reduced the number of defects by softening the borosilicate to allow for a reorganization of the surface. As a result, the annealed borosilicate is essentially defect free and very flat[56]. In the case of the fused quartz, prior cleaning and experimentation have resulted in a rough surface with many large defects, as seen from the AFM data. As the quartz is not heated to its annealing temperature, the surface retains its roughness through the cleaning process. However, both the borosilicate and quartz surfaces display large numbers of surface silanol groups and are therefore chemically similar[79]. Mica is a naturally occurring mineral whose surface also displays silanol groups, but like the annealed borosilicate, the mica also additional atoms as part of its structure. Specifically, mica's structure contains potassium ions and aluminum as well as silicon and oxygen[80]. Physically, it is very similar to the annealed borosilicate glass, as the borosilicate glass is very flat and smooth from the annealing process and the freshly cleaved mica surface is characterized atomically flat with disperse terraces averaging 0.6 nm in height[81]. In contrast to these surfaces, the BSA surface is chemically unique as it is composed of denatured protein, presenting a variety of amino acid groups which are able to interact with the bilayer. Physically, it is rougher than either the annealed borosilicate or mica surface, though not as rough as the quartz surface[82]. At the concentration used, the denatured BSA is known to form in the mushroom regime[69].

We seek to understand how the substrate roughness and chemical groups affect

the lipids of an SLB, particularly the lipids' mobility. As the bilayer needs to be in close proximity to the substrate for the van der Waals interactions to be effective, increasing substrate roughness may disrupt some of the interactions and result in a more quickly diffusing bilayer. The effect of the observed substrate topology on bilayer diffusion was therefore explored by comparing the FRAP data for the differing substrates. Shown in Figure 3.2 is the effect of temperature on bilayer diffusion for four substrates, annealed borosilicate glass, quartz glass, mica, and protein-passivated (BSA) glass.

As shown by the curves of diffusion at various temperatures, quartz and mica display increased diffusion rates relative to the annealed borosilicate. In terms of non-silanol groups present on the substrate surface, these three substrates could be ordered as such: mica surface with many silanol, aluminum, and other mineral groups; annealed borosilicate with primarily surface silanol groups present, though an additional number of boron groups may also be present; and quartz glass with only surface silanol groups present. This ordering does not match the observed trend, as both high and low silanol concentration of quartz and mica surfaces lead to increased diffusion relative to annealed borosilicate. As mentioned, the quartz glass used herein was much rougher than the annealed borosilicate. The increased roughness corresponds to a larger number of bilayer defects, which may be partially responsible for the increased bilayer diffusion on quartz. The mica, though smoother than the annealed borosilicate glass on the sheets, displays some number of step edges. Similar to bilayer defects on the quartz surface, these step edges may be responsible for the increased bilayer diffusion observed on the mica surface.

The FRAP results for the mica also showed very large error bars, even with many samples observed. It is plausible the large variance of the diffusion rate for

mica was a result of the variance in the number of step edges present, not only from one sample to the next, but also in the region bleached for the FRAP experiment. These results suggest the bilayer-surface interactions are highly dependent on the surface topology. The results do not, however, answer whether the diffusion is dependent on the number of defects or the surface area in contact with the bilayer. To explore the question of surface contact area, work was done with a rough, protein passivated surface in which direct interacts at specific points were present.

Interestingly, the BSA surface shows a decrease in diffusion rate relative to the annealed borosilicate. In fact, the bilayer remains relatively immobile until the temperature of the system is increased well above room temperature to approximately 30 °C. The highly hindered diffusion is surprising, since if the topology were the driving consideration for bilayer-substrate interactions, one would expect the rough BSA surface to have similar results to those of quartz glass and mica, as discussed. The slowed bilayer diffusion suggests that the interactions between the BSA amino acids and the bilayer are dominating, hence restricting the bilayer diffusion almost entirely. It is known that mobile bilayers will not form on a BSA surface if the concentration of BSA is above 0.3 mg/mL, as the vesicles will not rupture if the BSA is in a brush configuration[69]. It could therefore be suggested that the bilayer is relatively immobile on a BSA surface because the vesicles have not ruptured to form the bilayer at lower temperature; as the temperature increases, the vesicles rupture and the bilayer becomes mobile. However, this argument was not found incorrect as it implies a BSA-supported bilayer heated to help vesicle rupture then subsequently cooled below room temperature should then have a diffusion rate closer to 1 $\mu m^2 s^{-1}$. This was not the case, as the system could be systematically heated and cooled without hysteresis in the FRAP results at each temperature. Additionally, the diffusion rate was observed to increase gradually

with temperature, not to jump; if vesicles were fusing, the sample should be relatively immobile until a critical temperature wherein vesicles fused, at which point the diffusion rate would jump to a more normal value. The results instead suggest the highly hindered bilayer diffusion is a result of neither surface topology nor unruptured vesicles, but instead a result of the type and strength of the chemical interactions involved. As the temperature increases, the interactions, including the tightly constrained interstitial water and amino acid-lipid head group interactions, are broken, allowing the bilayer to diffuse more freely. The breaking of these interactions would be gradual with temperature and reversible with temperature, as was observed. This is an interesting result as it implies the bilayer-surface interaction for a POPC bilayer on a BSA passivated substrate is dominated by chemical interactions, not by surface structure or topology.

3.3.2 Impact of Bilayer Charge on Bilayer Diffusion

In addition to changing the substrate characteristics, the bilayer-substrate interaction can be modulated by tuning the bilayer characteristics. To explore the impact of the bilayer characteristics on the bilayer-substrate interactions, the diffusion of lipids in bilayers of varying lipid compositions were observed. First, the impact of the charge of the bilayer on bilayer-substrate interactions was investigated by altering the molar concentration of charged lipids in a bilayer formed on annealed borosilicate glass. Three compositions of bilayers are examined: a neutral bilayer composed of 99.5/0.5 mole% POPC/TR-DHPE, a positively charged bilayer composed of 10/89.5/0.5 mol% DOTAP/POPC/TR-DHPE, and a negatively charged bilayer composed of 10/89.5/0.5 mol% POPA/POPC/TR-DHPE. All three bilayer compositions were formed on annealed borosilicate. It should be noted all bilayers

referred to in this section were formed with 10 mM Tris buffer at pH 7.4 with 100 mM NaCl. Attempts were made to form the bilayers at lower salt concentration; unfortunately, the vesicles containing 10 mol% of the negatively charged lipid POPA would not fuse. Since the substrate carries a negative charge and POPA contains a negatively charged phosphate group, the higher ionic strength was necessary to screen the repulsive force for bilayer fusion to occur. The observed lipid bilayer diffusion of differently charged bilayers on annealed borosilicate is shown in Figure 3.3.

Based solely on the negative charge of the substrate, one would expect the negative bilayer to be electrostatically repulsed from the substrate, pushing it away and enhancing observed diffusion relative to a neutral bilayer; likewise, one would expect a positively charged bilayer to be electrostatically attracted to the substrate, bringing it closer and hindering diffusion relative to a neutral bilayer. Surprisingly, all three bilayers look similar both in the diffusion coefficients at room temperature as well as in impact on diffusion from temperature. This finding is contrary to expectations and suggests the interaction may not be solely resultant from the negative silanol groups coupling with the membrane. All SLBs were formed in ionic solutions and after bilayer fusion, some amount of salt remained in the interstitial water region, trapped between the bilayer and the substrate. The similarity of the three bilayers could therefore be a result of interstitial ions interacting with the bilayers.

The similarity of bilayer diffusion coefficients at various temperatures suggests the negatively charged bilayer containing POPA acts very similarly to the neutral POPC bilayer in terms of the interactions between the bilayer and the substrate. Additionally, both interactions have similar response to increasing temperature. The similarity between the POPC and POPA bilayers is likely a result of the

negative ζ potential of POPC bilayers[83]. Additionally, the dye used to visualize under fluorescent microscopy, TR-DHPE, carries a negative charge. Though the dye is only present at 0.5 mol%, the dye furthers the apparent negative charge of the bilayer.

As was suggested by changing the substrate identity, the interactions between the substrate and bilayer are more likely dependent on the surface structure than the identity, which implies the interaction is dominated by non-specific interactions. Hence, changing the charge of the bilayer to modulate electrostatic attraction or repulsion between the substrate and bilayer does not create a large difference in lipid diffusion at most temperatures. In the case of the POPC and 10 mol% POPA bilayers, the salt screens the electrostatic repulsion between the substrate and bilayer when vesicle fusion occurs, leaving some amount of salt present between the substrate and the bilayer. The results show this residual salt must mediate the interaction of the bilayer and substrate, screening the electrostatic repulsion and encouraging bilayer coupling.

Relative to the neutral POPC and negative POPA bilayers, a larger increase in diffusion with increasing temperature was observed for the positively charged DOTAP bilayer, though the DOTAP bilayer's diffusion coefficients also showed a much larger variance at elevated temperature. The larger change in the DOTAP containing bilayer diffusion with temperature suggest the interactions coupling it to the substrate are more temperature sensitive than those present between the substrate and a POPC or POPA containing bilayer. As stated above, a bilayer containing positive lipids is expected to interact more directly with the negatively charged substrate without the intervention of the salt. The direct bridging between a bilayer lipid and a substrate silanol would be expected to decrease the overall lipid diffusion. The diffusion of the DOTAP containing bilayer is instead

observed to either be approximately the same as that of the POPC and POPA bilayers or faster. The data suggests either interactions between a lipid bilayer and annealed borosilicate are dominated by non-specific interactions rather than by charge interactions, or the salt reduces the impact of the substrate charge on the bilayer coupling. However, the greater response of the interaction to increasing temperature for a DOTAP containing bilayer reveals there must be a difference between the interaction of a DOTAP containing bilayer and the interaction of a POPA or POPC containing bilayer.

3.3.3 Impact of Cholesterol on Bilayer Diffusion

To explore the impact of the flexibility of the bilayer and interaction points between the bilayer and substrate, cholesterol was added to POPC vesicles and bilayers were formed on both annealed borosilicate and BSA passivated glass. Cholesterol in a bilayer is known to change the bending elastic modulus of the bilayer by helping to fill in gaps in the tail region[84]. This change can decrease the diffusion of the lipids[85], as there is now a smaller free volume through which the lipids are able to slide by one other, thus decreasing the probability of such an event[86][87]. Additionally, the cholesterol stiffens the bilayer, increasing the difficulty for the bilayer to bend and follow the curvature and defects of a substrate. For a rough surface, the inability to follow the substrate would result in fewer points of interaction with the substrate, resulting in a competing effect and potentially increasing the observed diffusion. As seen for the annealed borosilicate glass, the lipid diffusion was slowed relative to the POPC bilayer. Because annealed borosilicate is relatively flat form the annealing process, the addition of cholesterol to the bilayer will decrease the lipid free volume but will have very little effect on the number

of contacts between the planar substrate and an already planar bilayer. As such, the decrease in observed lipid mobility with the addition of cholesterol was not surprising.

For the BSA-passivated surface, the interaction is not determined by surface roughness, as discussed. However, the surface is intrinsically much rougher than the bilayer formed on annealed borosilicate and the bilayer must conform to the substrate topology to form the lipid-amino acid interactions. When cholesterol is added and the bilayer can no longer conform, the total substrate-bilayer interactions are weakened. However, the decrease in free volume has a competing effect, as shown in Figure 3.4.

The change in free volume has a dominating effect on the bilayer diffusion compared to the overall substrate-bilayer interaction. Hence, the diffusion coefficient is observed to decrease as a function of cholesterol content. To further explore the decrease in diffusion with the addition of cholesterol, the data were fit to an exponential decay and the decay rates were extracted. The decay rates for the bilayers formed on annealed borosilicate and on BSA passivated glass were 8.54 and 10.85 mol$\%^{-1}$, respectively. The larger decay rate for the bilayer formed on a BSA passivated surface implies the bilayer is not as susceptible to changes in the cholesterol content as a bilayer formed on annealed borosilicate, though the data clearly show bilayers formed on both substrates are dominated by a slowing effect from the addition of cholesterol. The result suggests either the BSA somehow prevents the cholesterol from staying in the lipid bilayer, or a second effect is increasing lipid mobility.

As both bilayers were formed with identical compositions, the decrease in free volume with increasing cholesterol content should be the same. If only the free volume of the lipids were changing, the two bilayers would have the same decay

constant. As discussed, increasing the cholesterol composition also changes how the bilayer can morph to follow the shape of the substrate. The larger decay rate for the bilayer formed on BSA passivated glass suggests as well as decreasing the lipid free volume, the addition of cholesterol is changing a second aspect of the bilayer. Interestingly, this second aspect seems to result in an increased diffusion. As the cholesterol is known to affect the bending elastic modulus[88], it is possible the bilayer is stiffened such that the total amount of surface area in contact with the rough BSA surface is decreased. This effect would decrease the number of interactions between the BSA amino acids and the lipid head groups, resulting in a faster diffusing bilayer. Taken together, the data suggest the addition of cholesterol has a net slowing effect on bilayer diffusion, but bilayers formed on a BSA passivated substrate have a competing, quickening effect from a decrease in bilayer flexibility and number of surface contact points.

The work herein provides a method by which bilayer attributes may be modulated to achieve a desired condition. The data show the modulation of interaction is not highly dependent on bilayer charge up to 10 mol% charged lipid content. However, the change in bilayer-substrate interaction is shown to change more drastically with temperature for a positively charged bilayer than for a neutral or negatively charged bilayer. The addition of cholesterol is observed to slow the bilayer diffusion, an expected result due to the decrease in free volume in the lipid tails. Interestingly, cholesterol's effect on the bending modulus created a competing effect on a BSA passivated substrate. The decrease in the bilayer's ability to bend to the substrate topology reduced the amount of interaction with the substrate, as evident by the larger decay rate for a bilayer formed on the rough BSA compared to a bilayer formed on the flat annealed borosilicate.

3.3.4 Combined Salt-Substrate Impact on Bilayer Diffusion

Preparation of annealed borosilicate glass prior to use included a cleaning bath of diluted 7X detergent and annealing at 550 °C for 6 hours. The cleaning bath helped remove any residue, coatings, or other material on the glass surface. The annealing process had two purposes: further cleaning by burning off any organics remaining after the bath and annealing to flatten the glass and remove any defects. During the annealing process, surface silanol groups break from the substrate; upon cooling, new silanol groups are formed, though not necessarily in the same positions or as frequently[89]. The annealing process helps to standardize the amount of surface silanol groups, and combined with the other effects, helps create uniform glass for experiments.

To test the effect annealing has on the substrate and bilayer subsequently formed on the substrate, different batches of glass were cleaned in identical manner to the annealed borosilicate except the batches were not subjected to the annealing and were instead used directly after drying with nitrogen. The diffusion of bilayers formed on such surfaces varied depending on production batch, and the bilayers showed either normal diffusion, or in some cases, extremely hindered diffusion. Interestingly, this result is in conflict with Seu et al. who found bilayers formed on non-annealed samples to diffuse more quickly[90]. This work highlights the need for substrate standardization as batch variability can lead to vastly different bilayer formation. Figure 3.5 highlights the differences observable, as one batch of non-annealed borosilicate gave very hindered bilayer diffusion compared to the annealed borosilicate.

It should be noted that the modified free volume outlined in Chapter 2 was

also applied to the non-annealed borosilicate diffusion curve, as seen in Figure 3.6. Interestingly, the model was well able to predict the effect of temperature on lipid diffusion until the large increase in diffusion at 50 °C. The fit suggests up to 40 °C, the substrate-bilayer interactions change as expected with temperature. Between 40 and 50 °C, however, the substrate-bilayer interaction changes far more drastically, suggesting the breaking of some interaction. The bilayer is known to interact with surfaces through van der Waals forces[91]; the large change is explainable by a strong, second, temperature dependent interaction present between the bilayer and substrate. An Arrhenius plot was also made for the f_s calculated for this system. The fit suggested the activation energy to overcome the bilayer-substrate coupling was 33 kJ/mol. This energy is again consistent with the bilayer coupled to the substrate through a constrained water region, though the value is less than the energy calculated for annealed borosilicate.

Both glasses had bilayers formed with the same lipid composition and solution conditions, and the only notable difference in the preparation was the lack of an annealing step. One might argue the low diffusion values suggest the lipid vesicles have either incompletely or failed to fuse. However, this cannot be the case as upon heating, the bilayer increases in diffusion rate and reaches more expected values, albeit still slow for the experimental temperature. Additionally, the bilayer returns to abnormally low diffusion values upon cooling to lower temperatures, which shows the bilayer was fused prior to heating.

Interestingly, the extremely hindered diffusion was found dependent on the ionic strength of the buffer solution upon bilayer formation. That is to say the heavily hindered diffusion was observed below a given ionic strength. Formed above that critical ionic strength, the bilayer diffused as normal with no change in diffusion with additional salt. Additionally, the critical ionic strength varied

with substrate batch. As observed experimentally with 99.5/0.5 mol% POPC/TR-DHPE bilayers, some non-annealed borosilicate allowed the formation of a normal diffusing bilayer, even with no NaCl added to the buffer. Another batch required at least 25 mM NaCl before normal-diffusing bilayers were observed. A third batch, shown in Figure 3.5, formed a slow-diffusing bilayer even after the addition of 100 mM NaCl. A high concentration of salt (>1 M NaCl) is known to impact bilayer properties, including bilayer height and fluidity; however, at the relatively low ionic strength used herein, these direct interactions between the bilayer and salt are not expected[92]. Therefore, ions in the proximal water later must have a crucial role in bilayer diffusion on non-annealed borosilicate.

It is well known that the presence of ions in solution aid in the formation of the lipid bilayer[93]. As the negative potential vesicle comes in contact with the negatively charged substrate, electrostatic repulsion can hinder the interaction. Monovalent cations, such as sodium, can screen the charge repulsion; divalent cations, such as calcium, can bridge the two surfaces and aid in bilayer formation[94]. After bilayer formation, some salt must remain in the interfacial region between the bilayer and substrate and form interactions with both the bilayer and substrate[95], though little work has probed this salt directly. This work suggests the salt trapped in the interstitial water region plays a critical role in the normal diffusion of a supported bilayer. In addition to silicon dioxide and surface silanol groups, borosilicate glass has other atoms embedded in the structure and present on the surface, including boron, sodium, and aluminum; the amount of ions present on the surface must vary from one batch of glass to another. It is most logical to conclude the difference in required ionic strength arises from the difference in ions and non-silica based groups already present at the surface. These surface ions must be critical for bilayer diffusion; if a hypothetical bilayer has too

few ions present or available on its surface, a higher ionic strength must be required to trap more ions in the interstitial region between the lipid bilayer and surface and thus allow for normal diffusion.

As shown, the work herein indicates bilayer diffusion is dependent on ionic strength. While the importance of ionic strength on bilayer fusion is well documented, little evidence has shown ionic strength to impact the bilayer after formation[96]. This work challenges that assumption and shows a supported lipid bilayer requires a critical presence of ions for bilayers to diffuse normally. As an additional control, the identity of the salt was changed from NaCl to $CaCl_2$ for a POPC bilayer formed on annealed borosilicate, keeping the total ionic strength constant. Interestingly, the bilayer is found to diffuse independent of the salt identity. This finding suggests the interstitial and embedded non-silanol groups are not bridging between the bilayer and the substrate, as calcium would be expected to bridge much differently than sodium. Instead, the ions and groups are mediating the interaction in another way, possibly by creating a hydration shell barrier between the two surfaces. Unfortunately, such a barrier is very difficult to probe directly, as the number of molecules involved in such an interaction would be very small and would provide very little signal experimentally. Still, the work herein suggests a new way of considering the critical role of salt in mediating bilayer-substrate interactions.

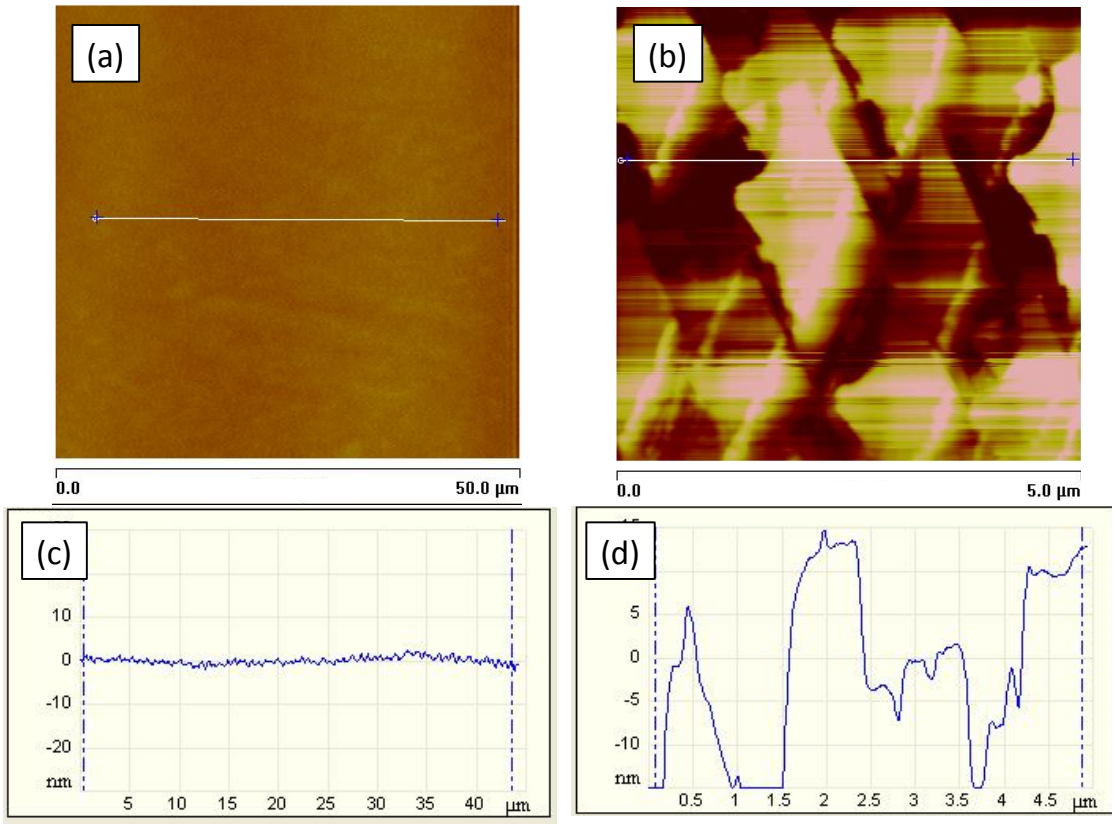

Surface	Annealed Glass	Non-Annealed Quartz
Roughness (Rms; nm)	0.48	9.26
Diffusion 23°C ($\mu m^2/s$)	1.45 ± 0.07	3.0 ± 0.4
Diffusion 40°C ($\mu m^2/s$)	4.2 ± 0.3	5.8 ± 0.5

Figure 3.1. Atomic Force Microscope Results for Substrates. The substrates examined were (a) annealed borosilicate float glass] and (b) fused quartz. Shown below the AFM images are the (c) line scan for the annealed borosilicate surface and (d) the line scan for quartz surface. Root-mean-square roughness as well as diffusion at 23 °C and 40 °C are also provide in the included table.

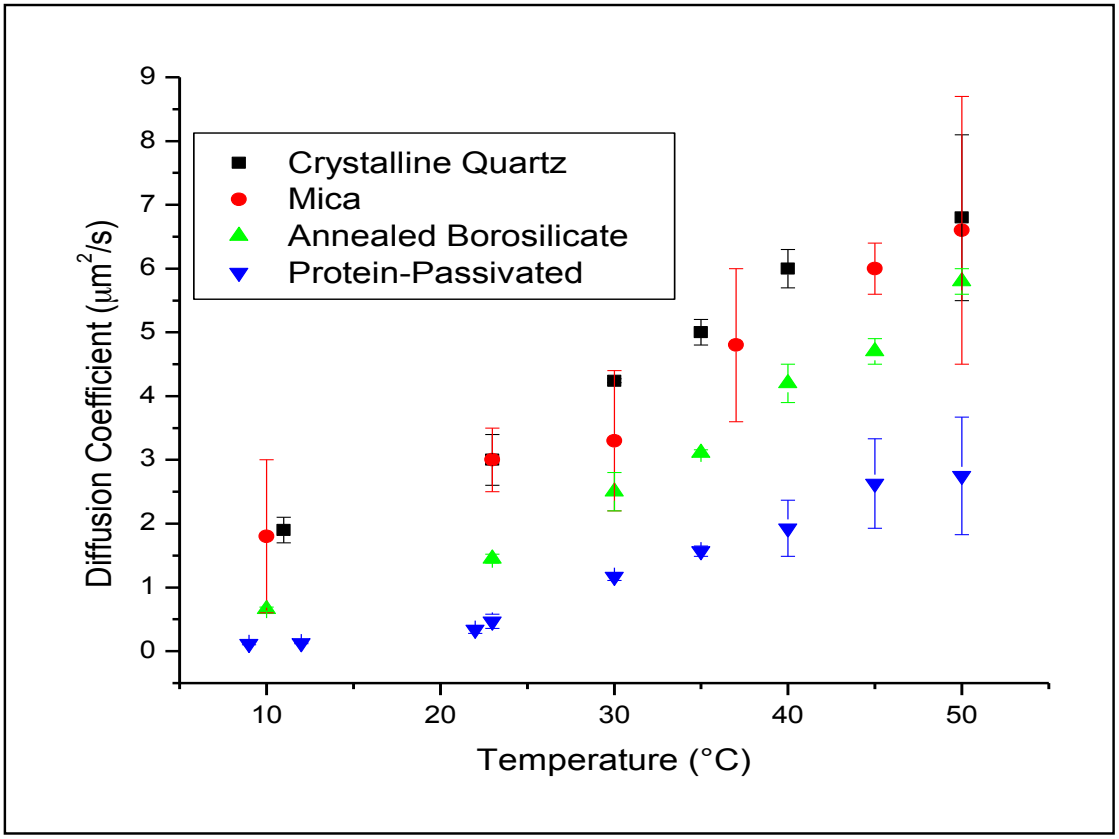

Figure 3.2. Temperature Dependent Diffusion of Bilayers Formed on Various Substrates. All bilayers were composed of 99.5 mol% POPC and 0.5 mol% TR-DHPE. Data is shown for bilayers formed on fused quartz (black square), mica (red circle), annealed borosilicate (green triangle), and protein-passivated surfaces (inverted blue triangle

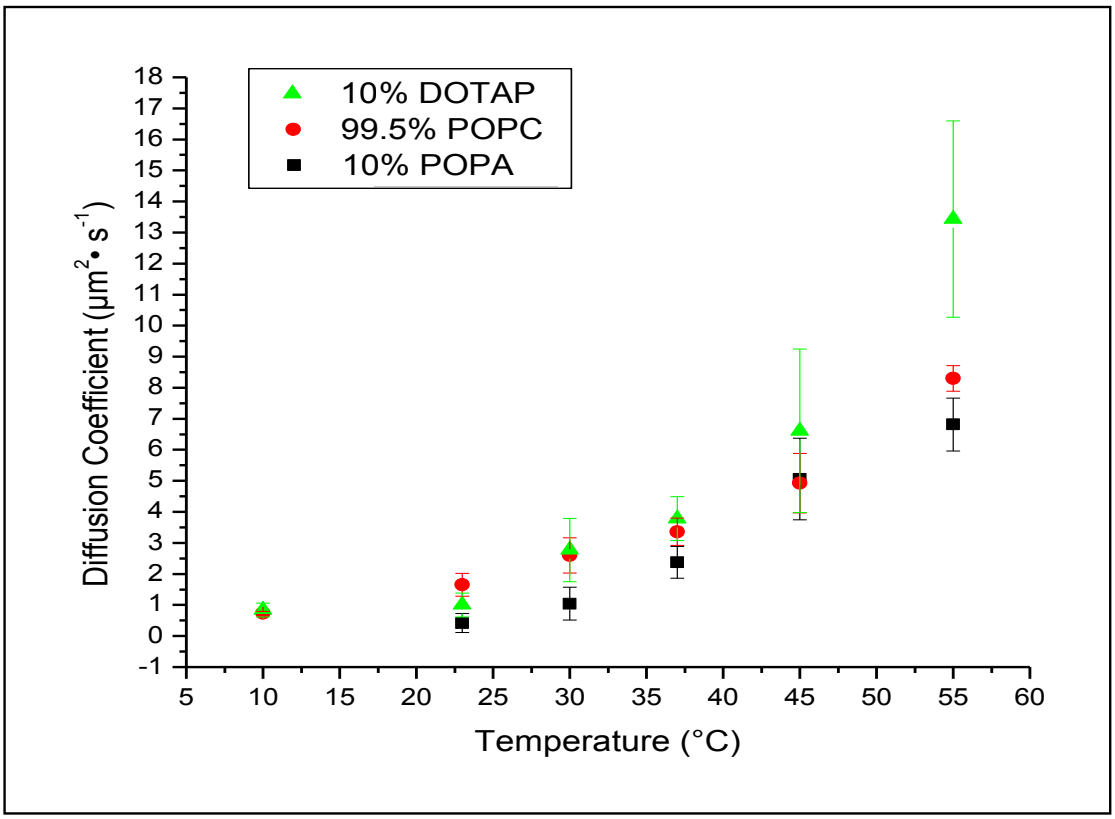

Figure 3.3. Diffusion-Temeperature Relationship for Charged Bilayers. For all bilayers, composition was 0.5mol% TR-DHPE, the desired amount of charged lipid, and the remaining mol% POPC. The three bilayers compared are as follows: a 10 mol% DOTAP bilayer (green triangle, positive charge), a strictly POPC bilayer with fluorescent dye (red circle, neutral charge), and a 10 mol% POPA bilaer (black square, negative charge)

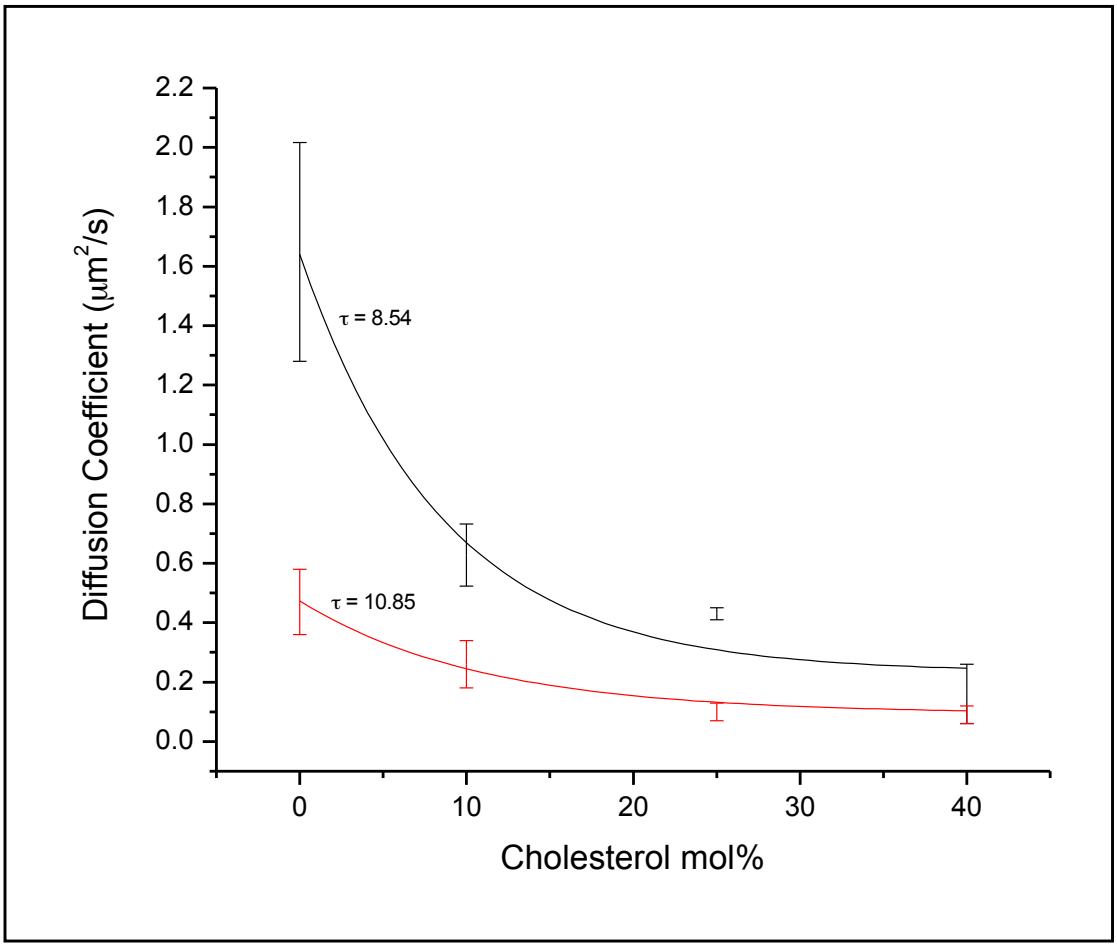

Figure 3.4. Impact of Cholesterol on Lipid Bilayer Diffusion. Shown are results for a POPC bilayer with 0.5 mol% TR-DHPE with varying amounts of cholesterol. Bilayers were formed on either annealed borosilicate glass (black) or protein-passivated glass (red).

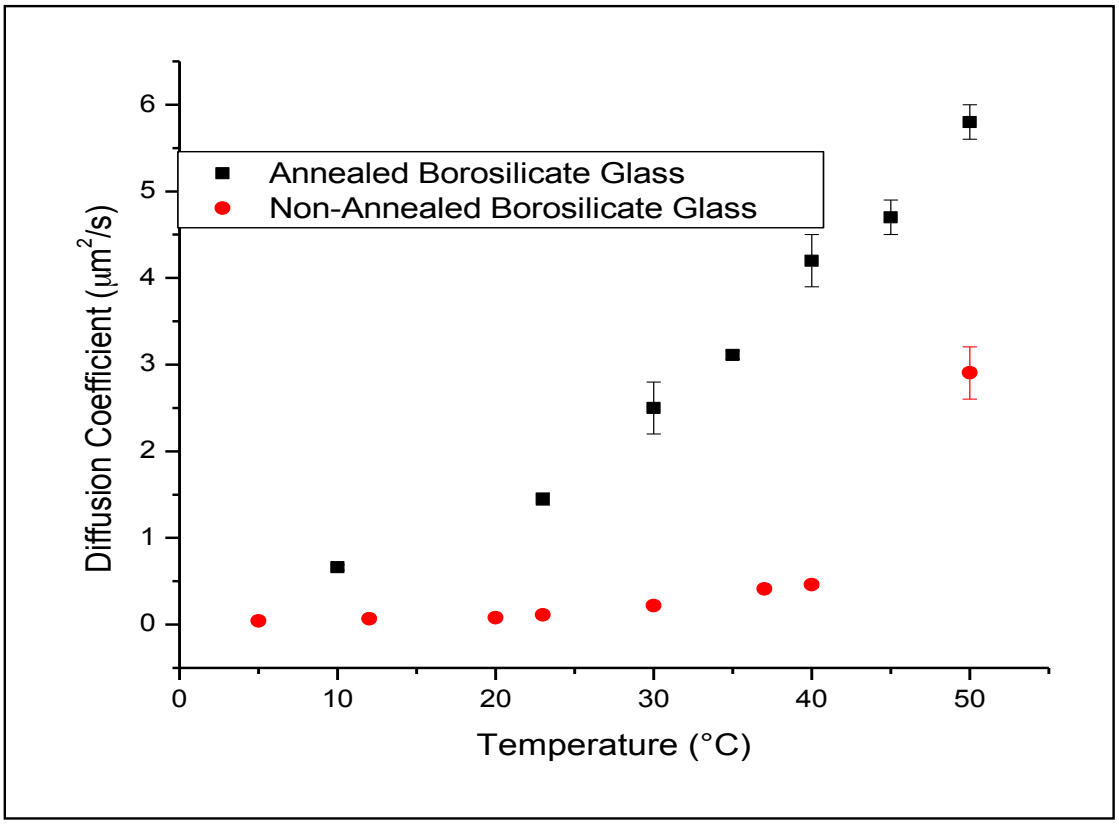

Figure 3.5. Effect of Annealing on Bilayer Diffusion. Shown are bilayers composed of 99.5 mol% POPC and 0.5 mol% TR-DHPE formed on either annealed borosilicate glass (black squares) or non-annealed borosilicate glass (red circles).

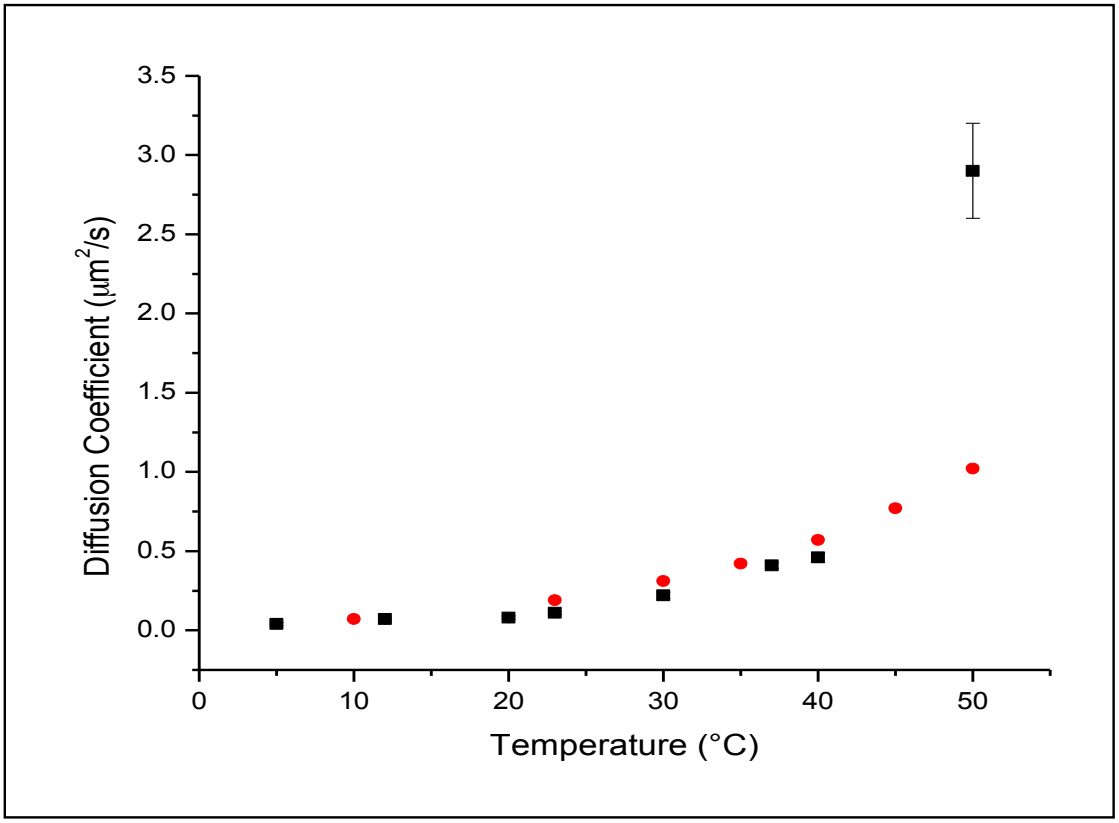

Figure 3.6. Non-Annealed FRAP Data Fit to a Modified Free Volume Model. Data for a 99.5/0.5 mol% POPC/TR-DHPE bilayer formed on non-annealed borosilicate glass (black square). The modified free volume model developed herein was applied to the data and the resultant predictions are shown (red circle).

Chapter 4

Aggregation of Lipid-Conjugated Dyes in Supported Lipid Bilayers

4.1 Introduction

Lipid bilayers form a protective barrier around cells to control the flow of nutrients and harmful materials as well to maintain gradients inside and outside of the cell[97]. These barriers are composed of many different types of lipids with a variety of characteristics, allowing the lipids to provide various functions including binding sites and maintaining membrane protein function[98][99][100][101]. Modulation of these lipids has also been explored to improve medical treatments, often through the disruption of bilayer functions, including ion permeability and bilayer fluidity[102][103][104][105]. Additionally, changes to the lipid environment, including temperature, have been shown to have an effect on the lipids and the bilayer[106][107][108]. To study properties of the membrane and its components, fluorescent dyes are often used to mark and track membrane bound proteins, peptides, and lipids, allowing for the direct visualization of the membrane through

fluorescence microscopy[109][110][111][112][113].

Because of its high quantum yield and stability, TR-DHPE is commonly used as a lipid conjugated dye. A Web of Science search of Texas Red shows 2,184 sources cite Texas Red as of May 2019. TR-DHPE belongs to the large class of dyes rhodamine, which includes rhodamine B and tetramethylrhodamine. Each dye has 19,267 and 1,308 citing references respectively as of May 2019. Some work has shown the presence of these dye-conjugated lipids can have an effect on the bilayer properties, including a broadening of the lipid phase transition[21][114]. However in many experiments, the effect of dye molecules, including TR-DHPE, is generally taken to be small or neglected. Additionally, the dye is assumed to not interact with other dye molecules because of the low molar concentration of dye used experimentally and the lack of observable self-quenching. When two dyes interact or are in close proximity to one another, studies have shown a resultant shift in the excitation and emission spectra of the dye, resulting of self-quenching of the signal[115]. TR-DHPE does not show significant self-quenching until above approximately 2 mol%, well above the concentrations used for most experiments[116]. As such, TR-DHPE has been assumed to be non-aggregated at experimental conditions.

Herein, we utilize a custom fluorescence microscope system to observe supported lipid bilayers at very low dye concentration. We note the presence of mobile, fluorescent bright spots in the bilayer and conclude the spots are dye aggregates based on bleaching events and diffusion. We further use the existence of aggregated dye to explain changes to the shape of the FRAP recovery curve with temperature.

4.2 Materials and Methods

4.2.1 Materials

Borosilicate glass microscope slides were purchased from Fisher Scientific (Hampton, NH). Sodium chloride salt was purchased from DOT Scientific Inc. (Burton, MI). Tris buffer salt was purchased from Calbiochem (San Diego, CA). PDMS was obtained from Dow Corning (Midland, MI) as Sylgard, silicone elastomer-184. A temperature-programmable circulator was obtained from VWR International (Radnor, PA).

POPC was purchased in chloroform from Avanti Polar Lipids, Inc. (Alabaster, AL). The lipid conjugated dye TR-DHPE in chloroform was obtained from Life Technologies (Grand Island, NY). The lipid conjugated dye 1-oleoyl-2-12-[(7-nitro-2-1,3-benzoxadiazol-4-yl) amino] dodecanoyl -sn- glycero -3- phosphoethanolamine (NBD-PE) in chloroform was purchased from Avanti Polar Lipids, inc. (Alabaster, AL). Atto 680 conjugated DOPE in chloroform was purchased from Atto Tec (Aalen, Germany).

Lipid extrusion was performed with a 10 mL LIPEX Extruder purchased from Northern Lipids Inc (Vancouver, Canada) using 200 nm Whatman track-etch membrane filters (Maidstone, United Kingdom).

4.2.2 Methods

Substrate Preparation

Borosilicate float glass cover slips were first cleaned in a 1:7 solution of 7X detergent and 18.2 MΩ water for 1.5 hours at 80 °C. Slides were then rinsed with copious amounts of 18.2 MΩ water and subsequently soaked in 18.2 MΩ water for

1.5 hours at 80 °C. Samples were again rinsed with 18.2 MΩ water and dried under a stream of nitrogen until all water was observed to have evaporated. Samples were further treated by annealing at 550 °C for 6 hours[56].

Lipid Vesicle Formation

Lipid vesicles were prepared by the freeze thaw extrusion method. POPC and TR-DHPE at 99.999/0.001 mol% respectively were mixed in chloroform then dried under nitrogen. The dried lipids were placed under vacuum for at least 2 hours to remove any residual chloroform. The lipid films were then rehydrated in buffer solution (100 mM NaCl, 10 mM Tris) at pH 7.4 to a lipid concentration of 1 mg/mL. The vial containing lipid solution was sonicated for 10 minutes to ensure rehydration of the lipids. The lipids spontaneously form multilamellar vesicles of varying size upon rehydration. The lipid solution was then put through 10 freeze thaw cycles by alternating liquid nitrogen and 80 °C water. The lipids were then extruded through a polycarbonate membrane with 200 nm pores[57]. The freeze thaw cycles and extrusion create unilammelar vesicles of consistent size. Vesicle size was confirmed by dynamic light scattering and the average vesicle size was approximately 130 nm.

Lipid Bilayer Formation

A PDMS well was placed atop the prepared substrate and 75 μL vesicle solution was added into the well. The vesicles were allowed 20 minutes for fusion to spontaneously occur. Excess lipids were then rinsed off with 18.2 MΩ water. A scratch made to the bilayer by gently running tweezers along the substrate and the bilayer was subsequently rinsed with excess 18.2 MΩ water. For bilayers formed at elevated temperature, the substrate and PDMS well were preheated and the temperature was maintained as the vesicle fusion occurred. Additionally for the

bilayers formed at elevated temperature, the sample was rinsed with the corresponding temperature 18.2 MΩ water prior to and after the scratch was made. For samples heated throughout the experiment or maintained at an elevated temperature, the PDMS well with the now formed lipid bilayer was then sealed by capping the well with a cleaned glass cover slide. Additional experiments were done wherein all rinsing steps were instead performed with buffer containing 100 mM NaCl and 10 mM Tris at pH 7.4; however, no difference was observed in experimental results.

Temperature Control

A hollow aluminum block with a circular hole in the center was connected to a temperature-programmable circulator (VWR). The aluminum block was placed on top of the sample, with the PDMS well inside the aluminum block's hole. Additionally, the hole in the aluminum block was covered to reduce temperature fluctuation. A thermocouple was used to monitor the bilayer temperature by measuring the substrate temperature on the side opposite to the bilayer. When the temperature was changed, a minimum of 30 minutes was allowed for re-equilibration at the new temperature.

Fluorescence Experiments

Fluorescent experiments were carried out on a Nikon Eclipse Ti inverted fluorescent microscope equipped with a 10X objective and a Hamamatsu C11440 CCD camera. The sample was illuminated with 561 nm light generated by an Aura II 4-NII-FA LED source. Sample bleaching was accomplished by a 561 nm laser generated by a Nikon LU-N3 laser box and directed by a Bruker Miniscanner.

Trajectory Analysis and Bleaching of Bright Spots

To record the bright spot trajectory, a 3 second video at 20 frames per second was captured. The trajectory analysis was carried out by the FIJI plugin Mosaic

Suite. To bleach the observed bright spots, a target circle roughly 30 μm in diameter was drawn and placed in the trajectory region of the mobile bright spot. A line scan was then taken across the bright spot and the peak intensity was recorded. The region was then bleached by a single pass hitting each pixel with a 5 mW 561 nm laser at a 100 μs dwell time. The peak intensity of the spot was then remeasured by line scan. The peak intensity measurement and bleaching event were alternated until the spot reached background fluorescence intensity.

Fluorescence Recovery After Photobleaching

A 30 μm diameter circle was bleached by targeting each pixel for 30 μs with an approximately 5 mW 532 nm laser. The laser would scan through the pixels, returning to the first after all pixels had been targeted, for a total of 3 seconds. Because both the time on each pixel and total bleaching time were small, the bilayer was taken to be evenly bleached in the bleaching area. This assumption was confirmed by a uniform, cylindrical bleaching profile as observed by a line scan of the bleaching area. The intensity of the bleached region was measured prior to and after bleaching and corrected to a similar, unbleached region of the bilayer. The spot intensity was monitored until full recovery was observed, as evident by the leveling off of the spot intensity. The bleached region intensity was normalized to an unbleached region of the bilayer and the percent recovery at a given time was calculated according to Equation 1.1. The fluorescence recovery as a function of time was plotted and fitted in one of two ways, either a single or a double exponential. For a single exponential fit, the data were fit to an exponential rise to maximum, as shown in Equation 1.2. The maximum at which the recovery leveled off is taken to represent the mobile fraction. For a double exponential fit, the data were fit according to Equation 4.1

$$F(t) = a(1 - e^{-bt}) + c(1 - e^{-dt}) \tag{4.1}$$

in which a second exponential component is added. The two terms a and c now represent the weights of two populations; the combination of a and c represents the mobile fraction of the sample. The exponential terms b and d are related to the $\tau_{1/2}$ for each population according to Equation 1.3. $\tau_{1/2}$ was in turn used to calculate two diffusion coefficients by utilizing Equation 1.4 for each population. In Equation 1.4, γ, the term enveloping the laser beam shape and intensity, was taken to be 1 due to its cylindrical bleach profile.

4.3 Results and Discussion

4.3.1 Dye Aggregation

At near-single molecule concentrations of dye, spots roughly four times the intensity of background fluorescence were observed. Interestingly, many of the spots were observed to be mobile. The number of bleaching laser pulses required to reduce intensity to background levels was recorded for each mobile fluorescent spot observed. Additionally, the diffusion coefficient was calculated for each spot; the correlation of the two parameters is shown in Figure 4.1.

As seen in the figure, the larger the number of bleaching events, the slower the diffusion coefficient. As multiple bleaching events imply multiple fluorescent molecules, it can be assumed the particles are dye aggregates. According to the Einstein-Stokes relationship, particle size and diffusion coefficient should be inversely proportional, a trend observed in the Figure 4.1. It should be noted all

bleached particles are assumed to be aggregates. The system contains a distribution of aggregate sizes; therefore, it is assumed there are also individual, non-aggregated fluorescent probes as well. These were not observed on the FRAP microscope setup, likely a result of low intensity relative to the aggregates. However, samples were view under 100x on a more sensitive microscope and a large number of previously undetected fast-diffusing molecules were observed. This agrees with the assumption smaller aggregates and non-aggregates were present but not observable by the FRAP microscope setup.

According to the Einstein-Stokes relationship, the relationship between diffusion coefficient and analyte radius should follow $D \propto -ln(a)$. Although the number of bleaching events is not precisely the radius of the aggregate, the data fits well to the trend. It stands to reason that the more bleaching events needed to bleach a spot would depend on the number of dye molecules present in the spot. As such, the more dye molecules present, the larger the assumed particle radius must be. This fit is further evidence the observed bright spots are aggregates, as a larger aggregate would have a larger radius in the membrane.

Some of the spots measured required only a single laser pulse to bleach to background intensity. Unfortunately, these points were difficult to track because they were moving quickly; as the particle would move across multiple pixels in a single exposure, the intensity was often spread across multiple pixels and the intensity would invariably fluctuate. The software used to track the particles and calculate diffusion coefficient would occasionally have frames where the particle was considered to have vanished. Constraints applied to continue tracking caused the diffusion values to have large error. As a result, the error bars for the spots requiring a single bleaching event are large.

There is also some ambiguity for the very slow diffusing particles requiring

more than 20 laser pulses to reach background intensity. The diffusion coefficients were near zero and the lack of movement makes it difficult to distinguish between very large aggregates and adsorbed, un-ruptured vesicles attached to the bilayer. It is assumed there is a mixture of very large aggregates and un-ruptured vesicles, though the trend remains unchanged with the inclusion of these questionable points.

A noteworthy characteristic of Texas Red is its ability to self quench. At high concentrations, the emission energy following photon absorption of one dye molecule can be absorbed by another dye molecule in very close proximity and lead to a non-radiative relaxation of the dye molecule. This effect is generally only seen when the dyes are forced into close proximity by high mole percent of the dye in the membrane[116]. If aggregates have indeed been observed in this system, the question as to why they are not self-quenching must inevitably follow. Some of the spots have displayed a notable increase in intensity following the initial bleaching event. It is plausible the dye molecules are quenching and once the initial bleaching event turns off some of the dyes, the dye molecules paired to a bleached dye now contribute to an overall increase in fluorescent intensity. Another possibility is of a lipid-mediated aggregation. Simulation data has suggested the dipoles of Texas Red and a PC head group can interact and form a relatively stable interaction[117]. This interaction may be further induced by the aforementioned mismatch between the large xanthene ring of TR-DHPE embedding into the predominantly POPC bilayer. The presence of these additional POPC lipids may help provide enough spacing to prevent the Texas Red from self-quenching.

4.3.2 Aggregate Size Influenced by Heating the Bilayer

Samples were then heated and the number of bleaching events required to completely bleach a particle was recorded and compared to the samples prior to heating, as shown in Figure 4.2. As observed, an increase in temperature decreases the distribution of bleaching steps required to reduce the bright spots to background intensity. This result is consistent with the claim the bright spots are aggregates, not simply non-ruptured vesicles.

If the particles are indeed aggregates, higher temperature should decrease the likelihood any two dye molecules will stick together; hence, aggregates should decrease as temperature increases. The result shows exactly the expected result for aggregates; that is, the aggregates have less fluorescent molecules at higher temperature and go through less intensity drops to reach background intensity. Additionally, the approximate number of spots observed at higher temperature was less than those observed at lower temperature, also suggesting the aggregates are smaller and less prevalent at high temperature.

4.3.3 Dependence of Dye Aggregation on Sample Preparation and Dye Characteristic

Additional preparation techniques were used to test if the observed aggregates were an artifact of sample preparation. In addition to the method involving serial dilution of known concentration of fluorescent probes, a contamination method and a tip sonication method were used. For the contamination method, vesicles containing no fluorescent dye (100 mol% POPC) were extruded through a membrane which had been previously used to extrude vesicles containing 99.5 mol% POPC and 0.5 mol% TR-DHPE. For the tip sonication method, vesicles prepared by serial

dilution of TR-DHPE were sonicated by a tip sonicator rather than a bath sonicator. Interestingly, none of the techniques increased or decreased the prevalence of observed spots. Additionally, the same aggregation properties were observed for all samples, indicating the aggregation is not a result of sample preparation but rather a characteristic of the fluorescent dye.

Other dyes were also used to confirm if this phenomenon was isolated to just TR-DHPE, to only xanthene based dyes, or ubiquitous for all dyes. To this end NBD-PE and Atto 680, whose structure is proprietary, were examined using the same procedure as used for TR-DHPE. All dyes used in this work showed mobile spots, though the amount and intensity of observed spots varied for each dye. This result is taken to indicate the aggregation is a general phenomenon of fluorescent dyes, possibly related to lipid mismatch[118].

4.3.4 Relating Aggregates to FRAP Data

FRAP data can be fit to an exponential growth function to retrieve information about the mobility of the lipids, particularly the diffusion coefficient and the mobile fraction, as shown through Equation 1.2. The recovery curve is often fit to a single exponential, as this provides a general description of the bilayer. However, the data clearly is not fully described by the single exponential, as seen in Figure 4.3. A double exponential matches the observed data well with much lower residuals than the single exponential fit. The double exponential fit suggests the presence of at least two diffusing populations present in the bilayer, though an even larger number of populations could be fit to the data. Based on the data shown previously, a bilayer has a distribution of aggregate sizes and therefore fits in theory to an exponential of an order matching the number of aggregate sizes. However, the

noise level of current FRAP techniques does not allow one to differentiate the higher order fits. In fact, even a third order fit does not greatly reduce the number of residuals relative to a second order fit. Therefore, the double exponential fit is considered sufficient for this technique. The slow diffusing population is considered representative of large, slow diffusing aggregates while the fast diffusing population is considered representative of the non-aggregated dye and small aggregates. As seen in Figure 4.4, the temperature of the system has a significant effect on the shape of the recovery curve.

At low temperature, the recovery of the slow population is more prominent, giving rise to a majority of the recovery occurring after 20 seconds. As temperature is increased, the recovery of the fast population becomes more prominent, giving rise to a large amount of recovery occurring between 0 and 20 seconds. This data suggests that as temperature increases, the dye shifts from being predominantly in larger aggregates (slow and immobile populations) to smaller aggregates and non-aggregated dye. The result is further confirmation the spots are indeed aggregates, and the result suggests that one can use temperature to control the level of aggregation. For experiments requiring the dye in a non or mostly non-aggregated environment, higher temperature is suggested. Working at a higher temperature will have the compounding effect of simplifying the recovery curve, as the high temperature curve fits well to a single exponential. As evident by the population fractions in Figure 4.4, even working at a biologically relevant temperature of 37 °C significantly decreases the impact of aggregation on the system.

In summary, the work shown herein shows direct visualization of lipid conjugated dye aggregation in a supported lipid bilayer system. Evidence supports the claim of aggregation based on the characteristics and behavior of the bright spots at very low lipid concentration. Additionally, the work provides a method

by which the level of aggregation may be controlled through temperature and dye selection. Although lipid-conjugated dye in a supported lipid bilayer is generally assumed to be individual dye molecules moving in a sea of lipids, this work clearly shows this is not the case. Dye aggregation should be considered in all fluorescent bilayer studies, especially those run at ambient temperature.

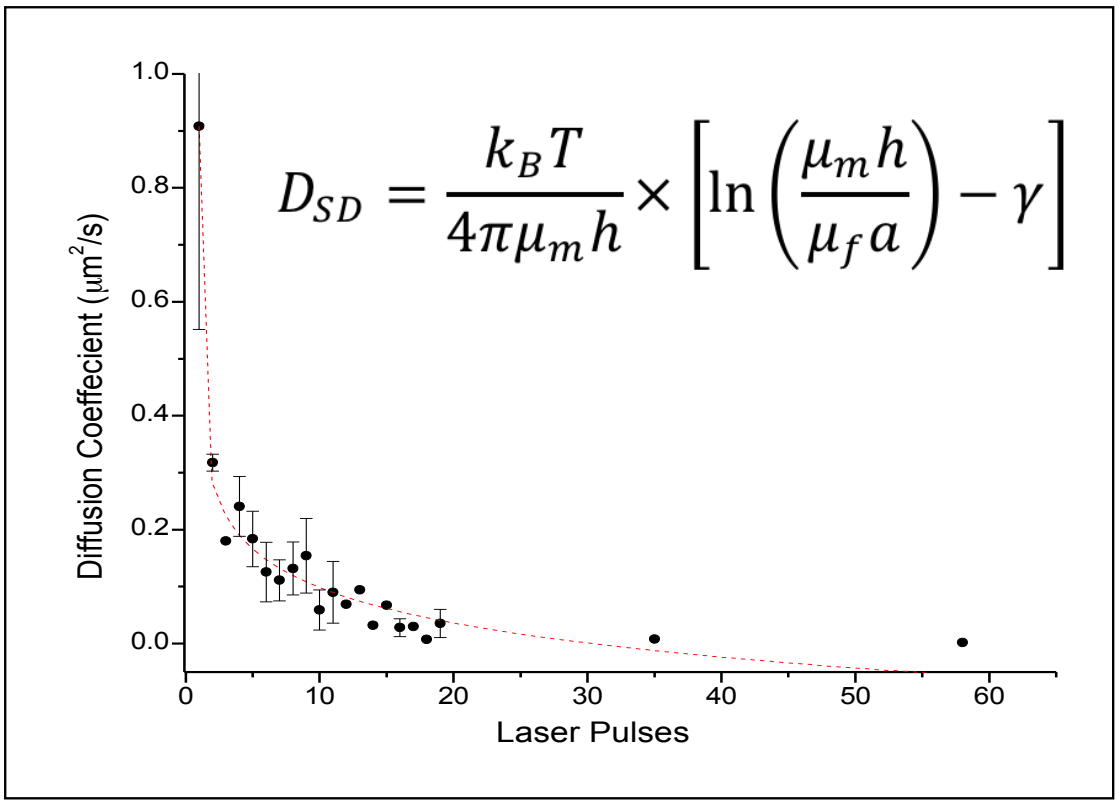

Figure 4.1. Diffusion Coefficient versus Number of Bleaching Events. The red line is the data fit to $f(y) = -A \cdot ln(x)$. Inset to the graph is the Saffman-Delbrück equation relating diffusion to particle size.

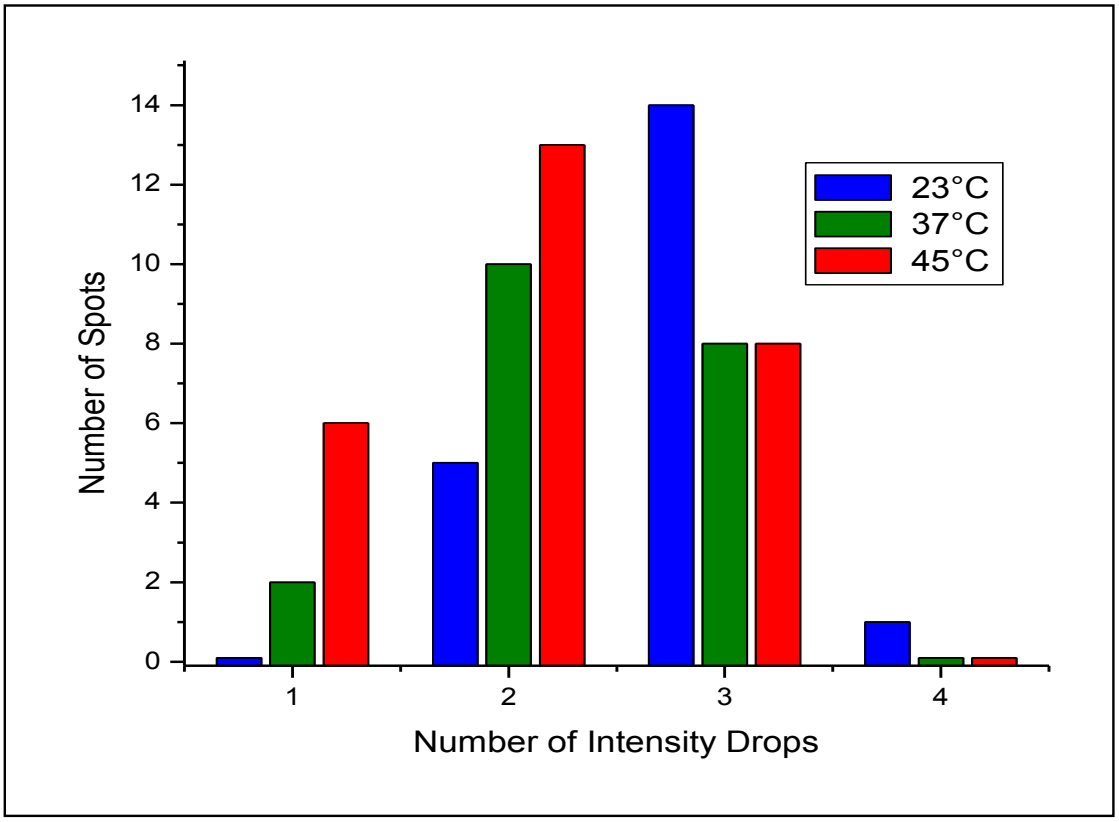

Figure 4.2. Impact of Heat on Aggregate Bleaching. Shown are the number of spots which required a certain number of intensity drops to reach background fluorescence intensity for spots observed at 23 °C (blue), 37 °C (green), and 45 °C (red).

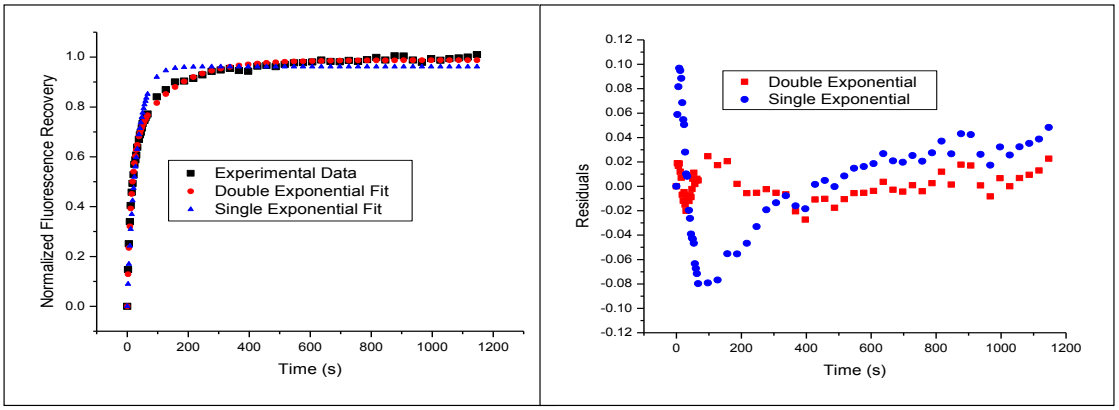

Figure 4.3. FRAP Recovery Curve Fit to a Single and Double Exponential. Fitting results are for a 99.5 mol% POPC and 0.5 mol% TR-DHPE bilayer formed on annealed borosilicate at 40 °C. Shown on the left are experimental data (black square), a double exponential fit (red circle), and a single exponential fit (blue triangle). Shown on the right are the residuals from the double exponential fit (red square) and the single exponential fit (blue circle).

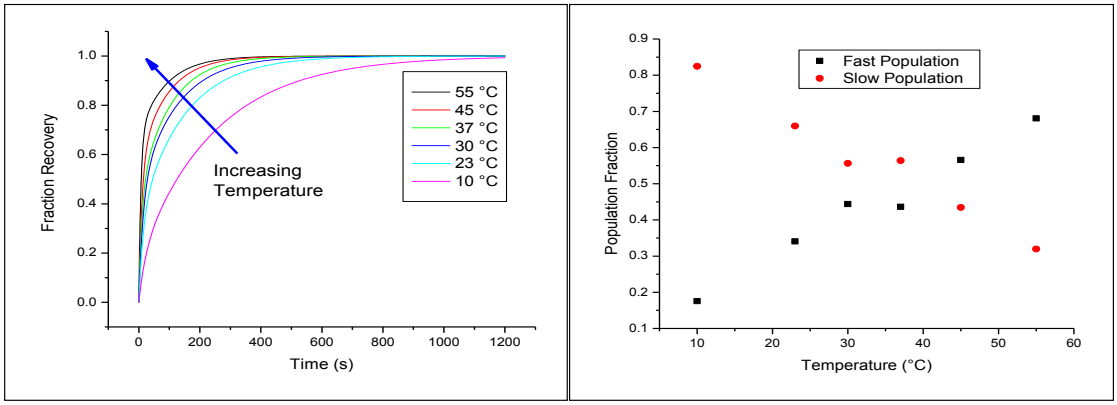

Figure 4.4. FRAP Recovery Curves and Population Fraction as a Function of Temperature. Shown are fitting results for a 99.5 mol% POPC and 0.5 mol% TR-DHPE bilayer formed on annealed borosilicate. Average FRAP recovery curves were each fit to a double exponential. From the fit, the fast diffusing (black) and slow diffusing (red) population fraction were obtained.

Chapter 5

Applications of Fluorescence Recovery After Photobleaching to Water Filtration Membranes

5.1 Introduction

Beyond studying the characteristics of the phospholipid bilayer, SLBs can be a useful tool to understand other particles either associated with the bilayer or embedded directly into the membrane[119][120]. The presence of these additional particles can cause measurable and observable changes to the bilayer, allowing deduction of how a particle may function or may be arranged within the bilayer[121][122]. This same approach may be extended even beyond phospholipid bilayers, as the same characteristics and qualities apply to synthetic systems, particularly to block copolymer systems[123][124].

Block copolymer bilayers are designed to be structurally very similar to phospholipid bilayers[125]. The two regions of the bilayer exposed to water are the polar

head region and the hydrophobic tail region[126]. In a phospholipid bilayer, the head group could be a phosphatidylcholine or a phosphatidylethanolamine, the two most biologically common head groups[127]. In a block copolymer, this could be any polar polymer chain, including poly(2-methyloxazolin) or polylactide[128][129]. The part of the bilayer hidden from the water is the nonpolar tail region. In a phospholipid bilayer, this could be any number of carbon chains, though biologically the chains are generally 16 or 18 carbons in length[130]. The chains may also differ in terms of the degrees of unsaturation depending on the purpose of the bilayer or the packing of additional components[131]. In a block copolymer bilayer, this tail region would be occupied by a nonpolar chain, such as polydimethylsiloxane and polybenzoxazole[132][133].

The advantage of a phospholipid bilayer is the mimicry of a living cell. As such, phospholipid bilayers are used heavily in biological studies. The advantage of a synthetic bilayer is the ability to easily customize the bilayer as well as resistance to or susceptibility to degradation[134][135]. If certain binding cites are desirable on the copolymer bilayer, the polymer head region can easily be modified; if a taller or shorter bilayer is desirable, the length of the head and tail region can be adjusted. Because of this high level of customization, synthetic block copolymer bilayers are often favored in industrial and biological applications[136][137][138].

Herein is discussed how fluorescence microscopy was utilized to understand and characterize the functionality and aggregation of synthetic, aquaporin-like water channels in both block copolymer and phospholipid membranes.

5.2 Materials and Methods

5.2.1 Materials

Pillar[5]arene channels (PAP channels) and Poly(butadiene)-*b*-poly(ethylene oxide) (PB-PEO) block copolymers were prepared was synthesized by Shen using previously published methods[139][140].

Peptide-appended hybrid[4]arene (PAH[4]) channels were synthesized by Song according to a combined procedure proposed by literature inolving the synthesis of hybrid[4]arene macrocyles followed by subsequent appending of the hybrid[4]arene with phenylalanine tripeptide (D-Phe-L-Phe-D-Phe-COOH, triPhe) side chains[141][84].

NBD-PE, POPC, and 1- palmitoyl- 2- oleoyl- *sn*- glycero- 3- phospho-L-serine (POPS) were purchased from Avanti Polar Lipids, Inc. (Alabaster, AL) and used without any further purification. TR-DHPE was obtained from Life Technologies (Grand Island, NY) and used without any further purification.

Borosilicate float glass was purchased from Fisher Scientific (Hampton, NH) and prepared by cleaning and annealing, further described below. PDMS was obtained from Dow Corning (Midland, MI) as Sylgard, silicone elastomer-184.

5.2.2 Methods

Substrate Preparation

Borosilicate float glass cover slips were first cleaned in a 1:7 dilute solution of 7X detergent and 18.2 MΩ water for 1.5 hours at 80 °C. Slides were then rinsed with copious amounts of 18.2 MΩ water and soaked in 18.2 MΩ water for 1.5 hours at 80 °C. The slides were then dried under a stream of nitrogen until all

water was evaporated, approximately 5 minutes. Glass slides were further treated by annealing at 550 °C for 6 hours[56].

PAP Channel in PB-PEO Vesicle Preparation

For experiments involving the PAP channel in PB-PEO block copolymer bilayers, vesicles were prepared by the film rehydration method[142]. PAP channels were added at 0.5 mol% to PB-PEO block copolymers in chloroform. For experiments requiring the visualization of the PAP channels, the channels were labelled with 5-(and-6)- ((N- (5-aminopentyl) amino) carbonyl) tetramethylrhodamine. For experiments requiring the visualization of bilayer, 0.5 mol% NBD-PE was added. Mixtures were dried on a rotary evaporator, then placed under high vacuum to remove any residual chloroform. The resultant polymer cakes were re-suspended in buffer containing 10 mM Hepes, 100 mM PEG600, and 0.01% (w/v) NaN_3 at pH 7 and left overnight on a stir plate at 4 °C. Vesicles were subsequently frozen and thawed ten times, followed by extrusion through a membrane with 200 nm pores ten times. Vesicle size was confirmed by dynamic light scattering.

PAH[4] Channel in Lipid Vesicle Preparation

For experiments involving the PAH[4] channel in lipid bilayers, vesicles were prepared by the film rehydration method[142]. PAH[4] channels were added to a POPS and POPC mixture at the desired ratio (0.5:20:79.5 PAH[4]:POPS:POPC) in chloroform. Channels were fluorescently labeled with 5- (and-6)- ((N- (5-aminopentyl) amino) carbonyl) tetramethylrhodamine to track the channel diffusion. Mixtures were dried on a rotary evaporator, then placed under high vacuum to remove any residual chloroform. Lipid cakes were re-suspended in buffer containing 10 mM Hepes, 100 mM PEG600, and 0.01% (w/v) NaN_3 at pH 7 and left overnight on a stir plate at 4 °C. Vesicles were subsequently frozen and thawed ten

times, followed by extrusion through a membrane with 200 nm pores fifteen times. Vesicle size was confirmed by dynamic light scattering.

Additional vesicles were made using non-labeled PAH[4] channels and TR-DHPE to assess the bilayer fluidity in the presence of channels. TR-DHPE and PAH[4] channels were added to a POPS, POPC mixture at the desired ratio (0.5:0.5:20:79.5 TR-DHPE:PAH[4]:POPS:POPC) in chloroform. Mixtures were then dried on a rotary evaporator, then placed under high vacuum to remove any residual chloroform. Lipid cakes were then re-suspended in buffer containing 10 mM Hepes, 100 mM PEG600, 0.01% (w/v) NaN_3 at pH 7 and left overnight on a stir plate at 4 °C. Vesicles were subsequently frozen and thawed ten times, followed by extrusion through a membrane with 200 nm pores ten times. Vesicle size was confirmed by dynamic light scattering.

Bilayer Formation

A PDMS well was placed on annealed borosilicate glass. Vesicle solution was added into the well and allowed to fuse for either 30 minutes (PAP channel) or 10 minutes (PAH[4] channel). After fusing, unruptured vesicles were rinsed off with buffer. Tweezers were then gently run along the substrate's surface to remove a line of bilayer material, providing contrast for fluorescent imaging. The surface was again rinsed with buffer and was capped with a clean glass slide.

Fluorescence Recovery After Photobleaching

Fluorescence recovery after photobleaching (FRAP) was performed on a home-built system including a Nikon Eclipse TE2000-U microscope with an X-Cite Series 120 halogen light source. Bleaching of the labelled lipid was accomplished with an Opto Engine LLC MBL-III-473 20 mW 473 laser with a DPSSL Driver power source. Bleaching of the labelled channel was accomplished with an Opto Engine

LLC MGL-III-532 300 mW 532 nm laser with a PSU-III-FDA power source. Power for each laser was reduced in the optical train to approximately 5 mW at the microscope stage. Sample was exposed to the laser for approximately 2 seconds for the initial bleaching event. Fluorescence intensity was monitored in the bleached region and normalized to a similar, unbleached region of the bilayer. Fluorescence recovery at a given time was then calculated according to Equation 1.1. The maximum at which the recovery leveled off is taken to represent the mobile fraction. For a double exponential fit, the data were fit according to Equation 4.1. $\tau_{1/2}$ was calculated for each population according to Equation 1.3. $\tau_{1/2}$ was in turn used to calculate two diffusion coefficients by utilizing Equation 1.4 for each population. In Equation 1.4, γ, the term enveloping the laser beam profile, was taken to be 0.88 for this microscope configuration.

5.3 Results and Discussion

5.3.1 Diffusion of PAP Channels in Synthetic Bilayers

To create a more robust water filtration membrane, artificial water channels, PAP, were inserted in block copolymer membranes. As filtration membranes are generally formed over a solid, porous support, the fluidity of the block copolymer bilayer and embedded artificial water channel over annealed borosilicate glass was explored. As shown in Figure 5.1 taken from Shen et al.[143], the diffusion of the embedded PAP channels was very slow and not adequately described by a single exponential fit.

The double exponential fit revealed a faster diffusing population with a diffusion coefficient of 0.086 $\mu m^2/s$ as well as a slower diffusing population with a

diffusion coefficient of 0.0069 $\mu m^2/s$. Additionally, both diffusion coefficients show the labelled PAP channel's diffusion was much slower than expected for a like-sized particle. As discussed in Chapter 4, the need to fit FRAP data to a double exponential is indicative of aggregation of the diffusing particle. The aggregation of PAP channels was in agreement with other results from vesicle based experiments; this work confirmed a collective structure could also form in an SLB system. Notably, the fitting of fluorescence recovery to a double exponential does not necessarily require two aggregate size distributions. Instead, it suggest a distribution of aggregate sizes which can be adequately described by two average sizes.

Aggregation of the channels is important for water filtration, as more channels per unit area correlates to a higher water throughput per unit area. An aggregated, functional channel is therefore preferred as it results in lower operational pressures and cheaper, faster water filtration. Thus, this work was exciting as it was able to show highly packed artificial water channels in a robust artificial block copolymer membrane could be easily generated over a solid support.

5.3.2 FRAP Evidence of PAH[4] Channel Aggregation

Further work focused on a second artificial water channel, PAH[4], which obtained even higher water transport rates and ion selectivity than the PAP channel. Molecular dynamics simulations (MD) previously suggested these desirable characteristics were related to the assembly of the individual channels into complex aggregates of two or more channels, allowing for an unusual but highly effective and selective water transport chain. Providing experimental evidence for sub-micron aggregates can present a challenge as they are not easy to visualize in the membrane.

As explored in Chapter 4, we have provided a means by which aggregation can

be assessed using FRAP curve fitting. Fluorescence experiments were therefore used as a key experimental tool in support of the simulation's suggestion of aggregation. As seen in results taken from this work in Figure 5.2, the channel diffused both slowly and with a strong need to fit to a double exponential. In fact, if the time past 1200 seconds is included in the fit, an argument could be made for even a third population. This is highly indicative of a wide distribution of aggregate sizes.

Additionally, fitting the diffusion of a lipid-bound dye, TR-DHPE, reveals the bilayer itself has hindered diffusion. This finding is consistent with aggregates which are not exclusive, but instead form an extended network encompassing bilayer lipids, hindering diffusion and possibly trapping the bilayer lipids. These results are in agreement with the MD simulations results and provide experimental evidence in support of the model's claim.

The combination of theory and experimental data provide strong corroborating evidence and a fundamental explanation for the aggregation of artificial water channels. The collaboration shows new applications of FRAP, highlighting its ability to characterize the size of aggregates as well as the aggregates' impact on the bilayer in which they are embedded.

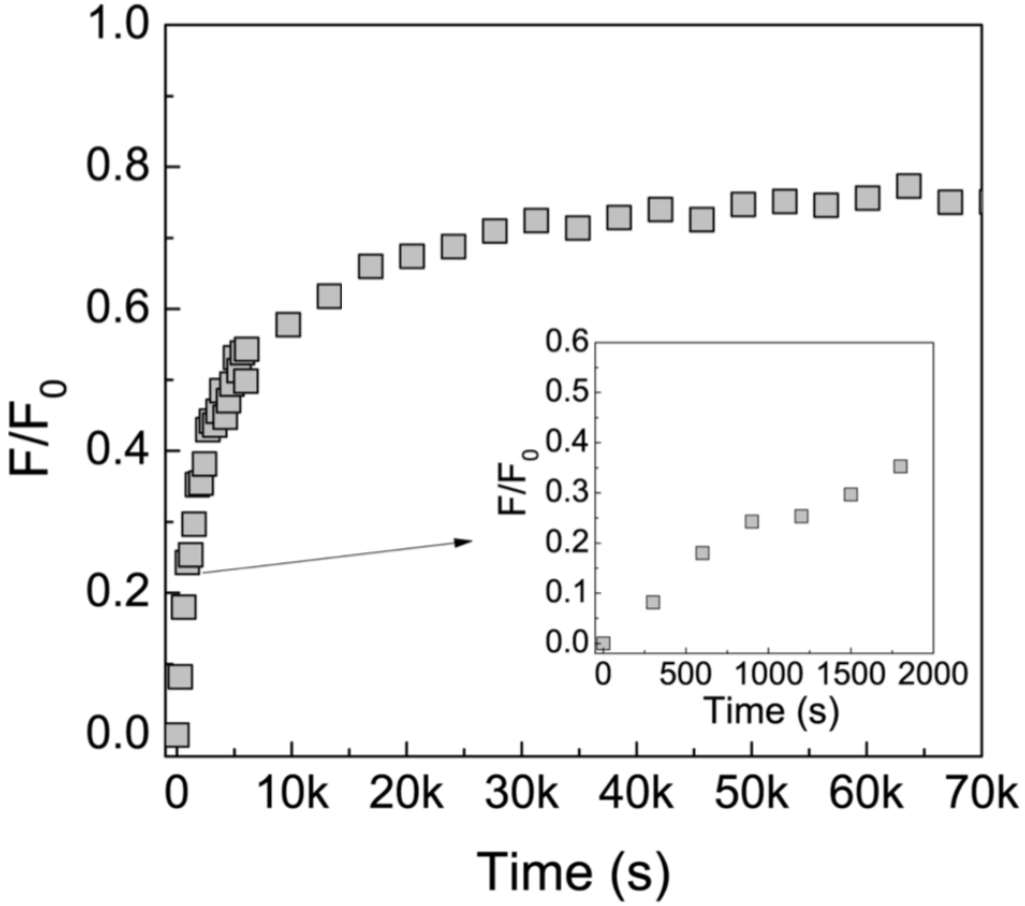

Figure 5.1. Fluorescence Recovery After Photobleaching of PAP Channel. A 0.5 mol% PAP channel in a PB-PEO diblock copolymer bilayer was formed over annealed borosilicate. Shown inset is the fluorescence recovery from the initial bleaching event to 2000 seconds for clarity.

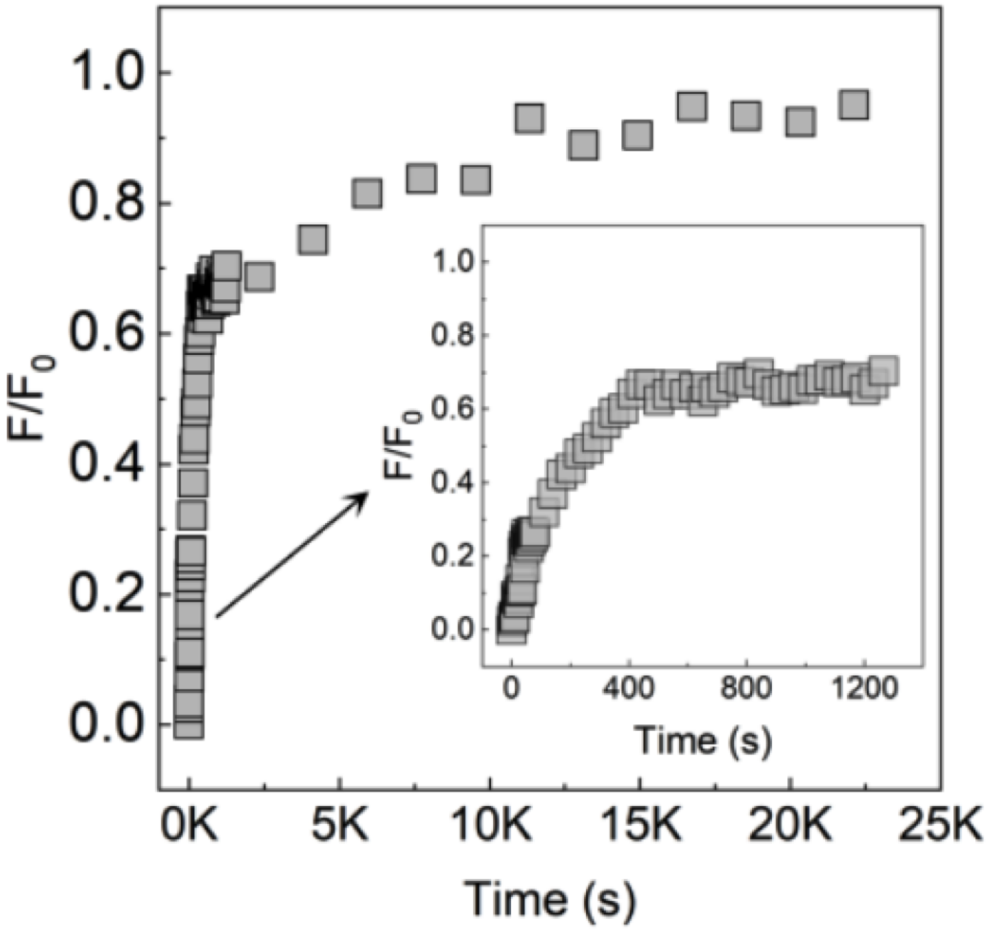

Figure 5.2. Fluorescence Recovery After Photobleaching of PAH[4] Channel. A 0.5:20:79.5 PAH[4]:POPS:POPC bilayer was formed over annealed borosilicate. Shown insert is the fluorescence recovery from the initial bleaching event to 1200 second.

Chapter 6

Conclusions

This dissertation has demonstrated a new model to describe the dynamic dependence on temperature for the diffusion of lipids in a supported lipid membrane. By modifying the extended free volume model to account for a change in the interaction between the lipid bilayer and the underlying substrate, a very good agreement to experimental results was obtained. This new model provided insights into the dominating factors affecting lipid diffusion. The model showed not only are the lipid volume, water friction, and intermembrane friction important, the drag of the bilayer over the substrate creates a crucial force to control lipid diffusion. This drag may be a result of the thin water layer or direct interactions between the bilayer and support.

The modified free volume model suggested methods to modulate the observed lipid diffusion. By changing the substrate, the impact of different interactions between the bilayer and the substrate were explored. A dependence on the substrate roughness was observed, where the number of close interaction points becomes important to describing the overall bilayer diffusion. This roughness dependence was further explored with cholesterol experiments to change the free volume of the

lipids and the bending elastic modulus of the bilayer. Additional ionic strength experiments showed the interesting behavior of some substrates, suggesting a critical role of salts in the ability of a lipid bilayer to flow over a substrate.

As suggested by the models, the diffusion of a particle was found dependent on the size of the particle. In the case of a simplistic model lipid membrane containing a small amount of fluorescent labelled lipids, aggregation was observed. This result was shown by a combination of photobleaching and particle tracking experiments and showed the dye-conjugated lipids will aggregate, even at very low concentration. Interestingly, the models suggest a distribution of aggregate sizes will result in a distribution of diffusion rates. The existence of a wide distribution of lipid diffusion provides a clear explanation for the need to fit FRAP curves to a double exponential.

Lastly, this dissertation showed applications lipid bilayers to industrially directed synthetic water filtration membranes. The same principles of diffusion and fluorescent microscopy were applied and provided insights into the presence, structure, and size of aquaporin-mimicking water channels. The results helped provide experimental evidence to support a molecular dynamics suggested mechanism for high water throughput. Additionally, the experiments offered an unusual application of FRAP, showcasing a simple method by which information about aggregation could be obtained without the use of expensive or time-consuming techniques.

The work shown herein has provided examples and evidence of how FRAP can be utilized to study a supported bilayer system. Though FRAP has a primary use in testing for bilayer formation, the work has proven FRAP is capable of exploring bilayer interactions and component aggregation. The development of a new model better describes the role of the support in an SLB provides a means by which temperature may be used to accurately control membrane fluidity. Exploration of

the impact of the support and membrane components provides methods by which a bilayer may be tuned to accomplish a specific condition. Justification for fitting FRAP data to a double exponential opens up the field to a method to simplify information about the mobility of membrane components, allowing for the isolation and study of a specific component. In total, this work has provided new insights into supported lipid bilayers and important new FRAP methodologies.

Bibliography

[1] Lucy, J. A. and A. M. Glauert (1967) "Assembly of Macromolecular Lipid Structures in Vitro," *Formation and Fate of Cell Organelles*, **6**, pp. 19–38.

[2] Huser, J. and L. A. Blatter (1999) "Fluctuations in Mitochondrial Membrane Potential Caused by Repetitive Gating of the Permeability Transition Pore," *Biochemical Journal*, **343**(2), pp. 311–317.

[3] Christensen, H. N. (1990) "Role of Amino Acid Transport and Countertransport in Nutition and Metabolism," *Physiological Reviews*, **70**(1), pp. 43–77.

[4] Huckabee, W. E. (1956) "Control of Concentration Gradients of Pyruvate and Lactate Across Cell Membranes in Blood," *Journal of Applied Physiology*, **9**(2), pp. 163–170.

[5] Hediger, M. A., M. F. Romero, J. B. Peng, A. Rolfs, H. Takanaga, and E. A. Bruford (2004) "The ABCs of Sulute Carriers: Physiological, Pathological and Therapeutic Implications of Human Membrane Transport Proteins," *Pflugers Archives*, **447**(5), pp. 465–468.

[6] Pawson, T. (1995) "Protein Modules and Signalling Networks," *Nature*, **373**(6515), pp. 573–580.

[7] Heldin, C. H., K. Miyazono, and P. T. Dijke (1997) "TGF-β Signalling from Cell Membrane to Nucleus Through SMAD Proteins," *Nature*, **390**(6695), pp. 465–471.

[8] Lingwood, D. and K. Simons (2010) "Lipid Rafts As a Membrane-Organizing Principle," *Science*, **327**(5961), pp. 46–50.

[9] Bakas, L., H. Ostolaza, W. L. C. Vaz, and F. M. Goni (1996) "Reversible Adsorption and Nonreversible Insertion of Escherichia coli α-Hemolysin into Lipid Bilayers," *Biophysical Journal*, **71**(4), pp. 1869–1876.

[10] Lundbaek, J. A., P. Birn, J. Girshman, A. J. Hansen, and O. S. Andersen (1996) "Membrane Stiffness and Channel Function," *Biochemistry*, **35**(12), pp. 3825–3830.

[11] Lundbaek, J. A. and O. S. Andersen (1994) "Lysophospholipids Modulate Channel Function by Altering the Mechanical Properties of Lipid Biayers," *Journal of General Physiology*, **104**(4), pp. 645–673.

[12] Gunning, P. W., G. Schevzov, A. J. Kee, and E. C. Hardeman (2005) "Tropomyosin Isoforms: Divining Rods for Actin Cytoskeleton Function," *Trends in Cell Biology*, **15**(6), pp. 333–341.

[13] Hall, A. (1998) "Rho GTPases and the Actin Cytoskeleton," *Science*, **279**(5350), pp. 509–514.

[14] Lee, M. H., D. A. Brass, R. Morris, R. J. Composto, and P. Ducheyne (2005) "The Effect of Non-Specific Interactions on Cellular Adhesion Using Model Surfaces," *Biomaterials*, **26**(14), pp. 1721–1730.

[15] O'Brien, J. S. (1967) "Cell Membranes-Composition: Structure: Function," *Journal of Theoretical Biology*, **15**(3), pp. 307–324.

[16] Marsh, D. (2013) *Handbook of Lipid Bilayers*, 2nd ed., CRC Press.

[17] Allen, M. J., E. M. Bradbury, and R. Balhorn (1997) "AFM Analysis of DNA-Protamine Complexes Bound to Mica," *Nucleic Acids Research*, **25**(11), pp. 2221–2226.

[18] Orhan, J. B., V. K. Parashar, J. Flueckiger, and M. A. M. Gijs (2008) "Internal Modification of Poly(dimethylsiloxane) Microchannels with a Borosilicate Glass Coating," *Langmuir*, **24**(16), pp. 9154–9161.

[19] Keller, C. A. and B. Kasemo (1998) "Surface Specific Kinetics of Lipid Vesicle Adsorption Measured with a Quartz Crystal Microbalance," *Biophysical Journal*, **75**(3), pp. 1397–1402.

[20] Yi, C., C. W. Li, S. Ji, and M. Yang (2006) "Microfluidics Technology for Manipulation and Analysis of Biological Cells," *Analytica Chimica Acta*, **560**(1), pp. 1–23.

[21] Bouvrais, H., T. Pott, L. A. Bagatolli, J. H. Ipsen, and P. Meleard (2010) "Impact of Membrane-Anchored Fluorescent Probes on the Mechanical Properties of Lipid Bilayers," *Biochimica et Biophysica Acta - Biomembranes*, **1798**(7), pp. 1333–1337.

[22] Galush, W. J., J. A. Nye, and J. T. Groves (2008) "Quantitative Fluorescence Microscopy Using Supported Lipid Bilayer Standards," *Biophysical Journal*, **95**(5), pp. 2512–2519.

[23] Lin, W. C., C. D. Blanchette, T. V. Ratto, and M. L. Longo (2006) "Lipid Asymmetry in DLPC/DSPC-Supported Lipid Bilayers: A Combined AFM and Fluorescence Microscopy Study," *Biophysical Journal*, **90**(1), pp. 228–237.

[24] Xie, X. S. and J. K. Trautman (1998) "Optical Studies of Single Molecules at Room Temperature," *Annual Review of Physical Chemistry*, **49**(1), pp. 441–480.

[25] Axelrod, D., D. Koppel, J. Schlessinger, E. Elson, and W. Webb (1976) "Mobility Measurement by Analysis of Fluorescence Photobleaching Recovery Kinetics," *Biophysical Journal*, **16**(9), pp. 1055–1069.

[26] Koppel, D. E., D. Axelrod, J. Schlessinger, and E. L. Elson (1976) "Dynamics of Fluorescence Marker Concentration as a Probe of Mobility," *Biophysical Journal*, **16**(11), pp. 1315–1329.

[27] Soumpasis, D. M. (1983) "Theoretical Analysis of Fluorescence Photobleaching Recovery Experiments," *Biophysical Journal*, **41**, pp. 95–97.

[28] Sprague, B. L. and J. G. McNally (2005) "FRAP Analysis of Binding: Proper and Fitting," *Trends in Cell Biology*, **15**(2), pp. 84–91.

[29] Sendecki, A. M., M. F. Poyton, A. J. Baxter, T. Yang, and P. S. Cremer (2017) "Supported Lipid Bilayers with Phosphatidylethanolamine as the Major Component," *Langmuir*, **33**, pp. 13423–13429.

[30] Singer, S. J. and G. L. Nicolson (1972) "The Fluid Mosaic Model of the Structure of Cell Membranes," *Science*, **175**(4023), pp. 720–731.

[31] Miller, C. C. (1924) "The Stokes-Einstein Law for Diffusion in Solution," *Proceedings of the Royal Society of London. Series A, Containing Papers of a Mathematical and Physical Character*, **106**(740), pp. 724–749.

[32] Tuteja, A., M. E. Mackay, S. Narayanan, S. Asokan, and M. S. Wong (2007) "Breakdown of the Continuum Stokes-Einstein Relation for Nanoparticle Diffusion," *Nano Letters*, **7**(5), pp. 1276–1281.

[33] Saffman, P. G. and M. Delbrück (1975) "Brownian Motion in Biological Membranes," *Proceedings of the National Academy of Science*, **72**, pp. 3111–3113.

[34] Vogele, M., J. Kofinger, and G. Hummer (2019) "Finite-Size-Corrected Rotational Diffusion Coefficients of Membrane Proteins and Carbon Nanotubes from Molecular Dynamics Simulations," *Journal of Physical Chemistry B*, **123**(24), pp. 5099–5106.

[35] Vaz, W. L. C., R. M. Clegg, and D. Hallmann (1985) "Translational Diffusion of Lipids in Liquid Crystalline Phase Phosphatidylcholine Multibilayers. A Comparison of Experiment with Theory," *Biochemistry*, **24**(3), pp. 781–786.

[36] Turnbull, D. and M. H. Cohen (1961) "Free-Volume Model of the Amorphous Phase: Glass Transition," *Journal of Chemical Physics*, **34**(1), pp. 120–125.

[37] Reviakine, I. and A. Brisson (2000) "Formation of Supported Phospholipid Bilayers from Unilamellar Vesicles Investigated by Atomic Force Microscopy," *Langmuir*, **16**(4), pp. 1806–1815.

[38] Alberts, B., A. Johnson, J. Lewis, M. Raff, K. Roberts, and P. Walter (2002) *Molecular Biology of the Cell*, 4th ed., Garland Science, New York.

[39] Cho, W. and R. V. Stahelin (2005) "Membrane-Protein Interactions in Cell Signaling and Membrane Trafficking," *Annual Review of Biophysics & Biomolecular Structure*, **34**, pp. 119–151.

[40] Cooper, G. M. and R. E. Hausman (2000) *The Cell: A Molecular Approach*, 2nd ed., Sunderland (MA): Sinauer Associates.

[41] Ladha, S., A. R. Mackie, L. J. Harvey, D. C. Clark, E. J. Lea, M. Brullemans, and H. Duclohier (1996) "Lateral Diffusion in Planar Lipid Bilayers: A Fluorescence Recovery After Photobleaching Investigation of Its Modulation by Lipid Composition, Cholesterol, or Alamethicin Content and Divalent Cations," *Biophysical Journal*, **71**(3), pp. 1364–1373.

[42] Doyle, E. L., C. A. Hunter, H. C. Phillips, S. J. Webb, and N. H. Williams (2003) "Cooperative Binding at Lipid Bilayer Membrane Surfaces," *Journal of the American Chemical Society*, **125**(15), pp. 4593–4599.

[43] Monson, C. F., X. Cong, A. Robison, H. P. Pace, C. Liu, M. F. Poyton, and P. S. Cremer (2012) "Phosphatidylserine Reversibly Binds Cu^{2+} with Extremely High Affinity," *Journal of the American Chemical Society*, **134**, pp. 7773–7779.

[44] Avanti Polar Lipids (2019), "Lipid Products | 16:0-18:1 PC | 850457," Electronic.

[45] ——— (2019), "Lipid Products | 16:0 PC (DPPC) | 850335," Electronic.

[46] Berg, H. C. (1993) *Random Walks in Biology*, extended paperback ed., Princeton University Press, Princeton, NJ.

[47] Tamm, L. K. and H. M. McConnell (1985) "Supported Phospholipid Bilayers," *Biophysical Journal*, **47**, p. 105.

[48] Sonnleitner, A., G. J. Schütz, and T. H. Schmidt (1999) "Free Brownian Motion of Individual Lipid Molecules in Biomembranes," *Biophysical Journal*, **77**, p. 2638.

[49] Zhang, L. and S. Granick (2005) "Lipid Diffusion Compared in Outer and Inner Leaflets of Planar Supported Bilayers," *Journal of Chemical Physics*, **123**, p. 211104.

[50] Gennis, R. B. (1989) *Biomembranes: Molecular Structure and Function*, Springer.

[51] Reits, E. A. J. and J. J. NeefJes (2001) "From Fixed to FRAP: Measuring Protein Mobility and Activity in Living Cells," *Nature Cell Biology*, **3**, pp. E145–E147.

[52] Servedio, M. R., Y. Brandvain, S. Dhole, C. L. Fitzpatrick, E. E. Goldberg, C. A. Stern, J. V. Cleave, and D. J. Yeh (2014) "Not Just a Theory-The Utility of Mathematical Models in Evolutionary Biology," *PLoS Biology*, **12**(12), p. e1002017.

[53] Meier, K., A. Laesecke, and S. Kabelac (2004) "Transport Coefficients of the Lennard-Jones Model Fluid," *The Journal of Chemical Physics*, **12**(19), pp. 9526–9535.

[54] Kooijman, H. A. (2002) "A Modification of the Stokes-Einstein Equation for Diffusivities in Dilute Binary Mixtures," *Industrial & Engineering Chemistry Research*, **41**(13), pp. 3326–3328.

[55] Achuthan, S., B. J. Chung, P. Ghosh, V. Rangachari, and A. Vaidya (2011) "A Modified Stokes-Einstein Equation for A β Aggregation," *BMC Bioinformatics*, **12**(10), p. S13.

[56] Weissler, G. L. (1979) *Vacuum Physics and Tenchnology*, 2nd ed., Academic Press.

[57] Mayer, L. D., M. J. Hope, and P. R. Cullis (1986) "Vesicles of Variable Sizes Produced by a Rapid Extrusion Procedure," *Biochimica et Biophysica Acta - Biomembranes*, **858**, p. 161.

[58] Chaplin, M. F. (2007) "Water's Hydrogen Bond Strength," *arXiv Preprint Cond-Mat*, **0706**, p. 1355.

[59] Davson, H., J. F. Danielli, and E. N. Harvey (1943) *The Permeability of Natural Membranes*, The University Press.

[60] Yeagle, P. L. (1989) "Lipid Regulation of Cell Membrane Structure and Function," *The FASEB Journal*, **3**(7), pp. 1833–1842.

[61] Parpart, A. K. and A. J. Dziemian (1940) "The Chemical Composition of the Red Cell Membrane," *Cold Spring Harbor Symposia on Quantitative Biology*, **8**, pp. 17–24.

[62] McElhaney, R. N. and M. E. Tourtellotte (1969) "Mycoplasma Membrane Lipids: Variations in Fatty Acid Composition," *Science*, **164**(3878), pp. 433–434.

[63] Simons, K. and W. L. C. Vaz (2004) "Model Systems, Lipid Rafts, and Cell Membranes," *Annual Review of Biophysics & Biomolecular Structure*, **33**(1), pp. 269–295.

[64] Runas, K. A. and N. Malmstadt (2015) "Low Levels of Lipid Oxidation Radically Increase the Passive Permeability of Lipid Bilayers," *Soft Matter*, **11**, pp. 499–505.

[65] Sun, T. L., Y. Sun, C. C. Lee, and H. W. Huang (2013) "Membrane Permeability of Hydrocarbon-Cross-Linked Peptides," *Biophysical Journal*, **104**(9), pp. 1923–1932.

[66] Moran-Mirabal, J. M., J. B. Edel, G. D. Meyer, D. Throckmorton, A. K. Singh, and H. G. Craighead (2005) "Micrometer-Sized Supported Lipid Bilayers Arrays for Bacterial Toxin Binding Studies through Total Internal Reflection Fluorescence Microscopy," *Biophysical Journal*, **89**(1), pp. 296–305.

[67] Jonsson, M. P., P. Jonsson, A. B. Dahlin, and F. Hook (2007) "Supported Lipid Bilayer Formation and Lipid-Membrane-Mediated Biorecognition Reactions Studied with a New Nanoplasmonic Sensor Template," *Nano Letters*, **7**(11), pp. 3462–3468.

[68] Dietrich, C., L. A. Bagatolli, Z. N. Volovyk, N. L. Thompson, M. Levi, K. Jacobson, and E. Gratton (2001) "Lipid Rafts Reconstituted in Model Membranes," *Biophysical Journal*, **80**(3), pp. 1417–1428.

[69] Diaz, A. J., F. Albertorio, S. Daniel, and P. S. Cremer (2008) "Double Cushions Preserve Transmembrane Protein Mobility in Supported Bilayer Systems," *Langmuir*, **24**, pp. 6820–6826.

[70] Salafsky, J., J. T. Groves, and S. G. Boxer (1996) "Architecture and Function of Membrane Proteins in Planar Supported Bilayers: A Study with Photosynthetic Reaction Centers," *Biochemistry*, **35**(47), pp. 14773–14781.

[71] Litman, B. J. and D. C. Mitchell (1996) "A Role for Phospholipid Polyunsaturation in Modulating Membrane Protein Function," *Lipids*, **31**(1), pp. S193–S197.

[72] Guo, L., J. Y. Har, J. Sankaran, Y. Hong, B. Kannan, and T. Wohland (2008) "Molecular Diffusion Measurement in Lipid Bilayers over Wide Concentration Ranges: A Comparative Study," *Chem Phys Chem*, **9**(5), pp. 721–728.

[73] Kusumi, A., Y. Sako, and M. Yamamoto (1993) "Confined Lateral Diffusion of Membrane-Receptors as Studied by Single-Particle Tracking (Nanovid Microscopy) — Effects of Calcium-Induced Differentiation in Cultured Epithelial-Cells," *Biophysical Journal*, **65**, pp. 2021–2040.

[74] Eggeling, C., C. Ringemann, R. Medda, G. Schwarzmann, K. Sandhoff, S. Polyakova, V. N. Belov, B. Hein, C. von Middendorff, A. Schonle, and S. W. Hell (2009) "Direct Observation of the Nanoscale Dynamics of Membrane Lipids in a Living Cell," *Nature*, **457**(7233), pp. 1159–1162.

[75] Fujiwara, T., K. Ritchie, H. Murakoshi, K. Jacobson, and A. Kusumi (2002) "Phospholipids Undergo Hop Diffusion in Compartmentalized Cell Membrane," *Journal of Cell Biology*, **157**(6), pp. 1071–1081.

[76] Feder, T. J., I. Brust-Mascher, J. P. Slattery, B. Baird, and W. W. Webb (1996) "Constrained Diffusion or Immobile Fraction on Cell Surfaces: A New Interpretation," *Biophysical Journal*, **70**, pp. 2767–2773.

[77] de Laat, S. W., P. T. van der Saag, E. L. Elson, and J. Schlessinger (1980) "Lateral Diffusion of Membrane Lipids and Proteins During the Cell Cycle of Neuroblastoma Cells," *Proceedings of the National Academy of Science*, **77**(3), pp. 1526–1528.

[78] SCHOTT North America "Borosilicate Glass Properties," Electronic.

[79] Dijkstra, T. W., R. Duchateau, R. A. van Santen, A. Meetsma, and G. P. A. Yap (2002) "Silsesquioxane Models for Geminal Silica Surface Silanol Sites. A Spectroscopic Investigation of Different Types of Silanols." *Journal of the American Chemical Society*, **124**(33), pp. 9856–9864.

[80] Bampoulis, P., K. Sotthewes, M. H. Siekman, H. J. Zandvliet, and B. Poelsema (2017) "Graphical Visualizes the Ion Distribuiton on Air-Cleaved Mica," *Scientific Reports*, **7**, p. 43451.

[81] Ostendorf, F., C. Schmitz, S. Hirth, A. Kuhnle, J. J. Kolodziej, and M. Reichling (2008) "How Flat is an Air-Cleaved Mica Surface?" *Nanotechnology*, **19**(30), p. 305705.

[82] Silva-Lopez, E. I., L. E. Edens, A. O. Barden, D. J. Keller, and J. A. Brozik (2014) "Conditions for Liposome Adsorption and Bilayer formation on BSA Passivated Solid Supports," *Chemistry and Physics of Lipids*, **183**, pp. 91–99.

[83] Klasczyk, B., V. Knecht, R. Lipowsky, and R. Dimova (2010) "Interactions of Alkali Metal Chlorides with Phosphatidylcholine Vesicles," *Langmuir*, **26**(24), pp. 18951–18958.

[84] Chen, Z. and R. P. Rand (1997) "The Influence of Cholesterol on Phospholipid Membrane Curvature and Bending Elasticity," *Biophysical Journal*, **73**, pp. 267–276.

[85] Almeida, P. F. F., W. L. C. Vaz, and T. E. Thompson (1992) "Latteral Diffusion in the Liquid Phases of Dimyristoylphosphatidylcholine/Cholesterol Lipid Bilayers: A Free Volume Analysis," *Biochemistry*, **32**, pp. 6739–6747.

[86] Honerkamp-Smith, A. R., F. G. Woodhouse, V. Kantsler, and R. E. Goldstein (2013) "Membrane Viscosity Determined from Shear-Driven Flow in Giant Vesicles," *Physical Review Letters*, **111**, p. 038103.

[87] de Meyer, F. and B. Smit (2009) "Effect of Cholesterol on the Structure of a Phospholipid Bilayer," *Proceedings of the National Academy of Science*, **106**(10), pp. 3654–3658.

[88] Bochicchio, D. and L. Monticelli (2016) "The Membrane Bending Modulus in Experiments and Simulations: a Puzzling Picture," *Advances in Biomembranes and Lipid Self-Assembly*, **23**, pp. 117–143.

[89] Zhuravlev, L. T. (2000) "The Surface Chemistry of Amorphous Silica. Zhuravlev Model," *Colloids and Surfaces A: Physiochemical and Engineering Aspects*, **173**, pp. 1–38.

[90] Seu, K. J., A. P. Pandey, F. Haque, E. A. Proctor, A. E. Ribbe, and J. S. Hovis (2007) "Effect of Surface Treatment on Diffusion and Domain Formation in Supported Lipid Bilayers," *Biophysical Journal*, **92**(7), pp. 2445–2450.

[91] Israelachvili, J. N. (1994) "Strength of van der Waals Attration Between Lipid Bilayers," *Langmuir*, **10**(9), pp. 3369–3370.

[92] Pabst, G., A. Hodzic, K. Strancar, S. Danner, M. Rappolt, and P. Laggner (2007) "Rigidification of Neutral Lipid Bilayers in the Presense of Salts," *Biophysical Journal*, **93**(8), pp. 2688–2696.

[93] Cremer, P. S. and S. G. Boxer (1999) "Formation and Spreading of Lipid Bilayers on Planar Glass Supports," *Journal of Physical Chemistry B*, **103**(13), pp. 2554–2559.

[94] Cho, N. J., C. W. Frank, B. Kasemo, and F. Hook (2010) "Quartz Crystal Microbalance with Dissipation Monitoring of Supported Lipid Bilayers on Various Substrates," *Nature Protocols*, **5**(6), pp. 1096–1106.

[95] Richter, R. P. and A. R. Brisson (2005) "Following the Formation of Supported Lipid Bilayers on Mica: A Study Combining AFM, QCM-D, and Ellipsometry," *Biophysical Journal*, **88**(5), pp. 3422–3433.

[96] Richter, R. P., R. Berat, and A. R. Brisson (2006) "Formation of Solid Supported Lipid Bilayers: An Integrated View," *Langmuir*, **22**(8), pp. 3497–3505.

[97] Brown, D. H. and J. W. Bates (1990) "Bryophytes and Nutrient Cycling," *Botanical Journal of the Linnean Society*, **104**(1-3), pp. 129–147.

[98] Heron, D. S., M. Shinitzky, M. Hershkowitz, and D. Samuel (1980) "Lipid Fluidity Markedly Modulates the Binding of Serotonin to Mouse Brain Membranes," *Proceedings of the National Academy of Science*, **77**(12), pp. 7463–7467.

[99] Qin, L., C. Hiser, A. Mulichak, R. M. Garavito, and S. Ferguson-Miller (2006) "Identification of Conserved Lipid/Detergent Binding Sites in a High-Resolution Structure of the Membrane Protein Cytochrome C Oxidase," *Proceedings of the National Academy of Science*, **103**(44), pp. 16117–16122.

[100] Lundbaek, J. A., S. A. Collingswood, H. I. Ingolfsson, R. Kapoor, and O. S. Andersen (2009) "Lipid Bilayer regulation of Membrane Protein Function: Gramicidin Channels as Molecular Force Probes," *Journal of the Royal Society Interface*, **7**(44), pp. 373–395.

[101] Phillips, R., T. Ursell, P. Wiggins, and P. Sens (2009) "Emerging Roles for Lipids in Shaping Membrane-Protein Function," *Nature*, **459**(7245), pp. 379–385.

[102] Zalba, S. and T. L. M. ten Hagen (2017) "Cell Membrane Modulation as Adjuvant in Cancer Therapy," *Cancer Treatment Reviews*, **52**, pp. 48–57.

[103] Bosio, A., E. Binczek, and W. Stoffel (1996) "Functional Breakdown of the Lipid Bilayer of the Myelin Membrane in Central and Peripheral Nervous Systems by Disrupted Galactocerebrosidesynthesis," *Proceedings of the National Academy of Science*, **93**(23), pp. 13280–13285.

[104] Hendrich, A. B. and K. Michalak (2003) "Lipids as a Target for Drugs Modulating Multidrug Resistance of Cancer Cells," *Current Drug Targets*, **4**(1), pp. 23–30.

[105] Hurdle, J. G., A. J. O'neill, I. Chopra, and R. E. Lee (2011) "Targeting Bacterial Membrane Function: An Underexploited Mechanism for Treating Persistent Infections," *Nature Reviews. Microbiology*, **9**(1), pp. 62–75.

[106] Kucerka, N., M. P. Nieh, and J. Katsaras (2011) "Fluid Phase Lipid Areas and Bilayer Thickness of Commonly used Phosphatidylcholines as a Function of Temperature," *Biochemica et Biophysica Acta - Biomembranes*, **1808**(11), pp. 2761–2771.

[107] Liu, X. and B. Huang (2000) "Heat Stress Injury in Relation to Membrane Lipid Peroxidation in Creeping Bentgrass," *Crop Science*, **40**(2), pp. 503–510.

[108] Gates, R. D., G. Baghdasarian, and L. Muscatine (1992) "Temperature Stress Causes Host Cell Detachment in Symbiotic Cnidarians: Implications for Coral Bleaching," *The Biological Bulletin*, **182**(3), pp. 324–332.

[109] Shaner, N. C., R. E. Campbell, P. A. Steinbach, B. N. Giepmans, A. E. Palmer, and R. Y. Tsien (2004) "Improved Monomeric Red, Orange and Yellow Fluorescent Proteins Derived from Discosoma sp. Red Fluorescent Protein," *Nature Biotechnology*, **22**(12), pp. 1567–1572.

[110] Giepmans, B. N. G., S. R. Adams, M. H. Ellisman, and R. Y. Tsien (2006) "The Fluorescent Toolbox for Assessing Protein Location and Function," *Science*, **312**(5771), pp. 217–224.

[111] Pazos, E., O. Vazquez, J. L. Mascarenas, and M. E. Vazquez (2009) "Peptide-Based Fluorescent Biosensors," *Chemical Society Reviews*, **38**(12), pp. 3348–3359.

[112] Neef, A. B. and C. Schultz (2009) "Selective Fluorescence Labeling of Lipids in Living Cells," *Angewandte Chemie International Edition*, **48**(8), pp. 1498–1500.

[113] Nelson, N. and D. K. Schwartz (2018) "Single-Molecule Resolution of Antimicrobial Peptide Interactions with Supported Lipid A Bilayers," *Biophysical Journal*, **114**(11), pp. 2606–2616.

[114] Regan, D., J. Williams, F. Masia, P. Borri, and W. Langbein (2019) "Measuring Sub-Nanometer Thickness Changes During Phase Transitions of Supported Lipid Bilayers with Quantitative Differential Interference Contrast Microscopy," *Quantitative Phase Imaging V*, **10887**, p. 1088719.

[115] Bao, P., M. R. Cheetham, J. S. Roth, A. C. Blakeston, R. J. Bushby, and S. D. Evans (2012) "On-Chip Alternating Current Electrophoresis in Supported Lipid Bilayer Membranes," *Analytical Chemistry*, **84**(24), pp. 10702–10707.

[116] Groves, J. T. and S. G. Boxer (1995) "Electric Field-Induced Concentration Gradients in Planar Supported Bilayers," *Biophysical Journal*, **69**(5), pp. 1972–1975.

[117] Skaug, M. J., M. L. Longo, and R. Faller (2011) "The Impact of Texas Red on Lipid Bilayer Properties," *Journal of Physical Chemistry B*, **115**(26), pp. 8500–8505.

[118] Heberle, F. A., R. S. Petruzielo, J. Pan, P. Drazba, N. Kucerka, R. F. Standaert, G. W. Geigenson, and J. Katsaras (2013) "Bilayer Thickness Mismatch Controls Domain Size in Model Membranes," *Journal of the American Chemical Society*, **135**(18), pp. 6853–6859.

[119] Simons, K. and M. J. Gerl (2010) "Revitalizing Membrane Rafts: New Tools and Insights," *Nature Reviews. Molecular Cell Biology*, **11**(10), pp. 688–699.

[120] Seddon, A. M., P. Curnow, and P. J. Booth (2004) "Membrane Proteins, Lipids and Detergents: Not Just a Soap Opera," *Biochimica et Biophysica Acta - Biomembranes*, **1666**(1-2), pp. 105–117.

[121] Laganowsky, A., E. Reading, T. M. Allison, M. B. Ulmschneider, M. T. Degiacomi, A. J. Baldwin, and C. V. Robinson (2014) "Membrane Proteins Bind Lipids Selectively to Modulate Their Structure and Function," *Nature*, **510**(7503), pp. 172–180.

[122] Xie, J. X. (2006) *Lipid Dependent Topogenesis and Function of Membrane Proteins*, Ph.D. thesis, The University of Texas Graduate School of Biomedical Sciences, Houston, TX.

[123] Jackson, E. A. and M. A. Hillmyer (2010) "Nanoporous Membranes Derived from Block Copolymers: From Drug Delivery to Water Filtration," *ACS Nano*, **4**(7), pp. 3548–3553.

[124] Rosler, A., G. W. Vandermeulen, and H. A. Klok (2012) "Advanced Drug Delivery Devices Via Self-Assembly of Amphiphilic Block Copolymers," *Advanced Drug Delivery Reviews*, **64**(270-279).

[125] Mecke, A., C. Dittrich, and W. Meier (2006) "Biomimetic Membranes Designed from Amphiphilic Block Copolymers," *Soft Matter*, **2**(9), pp. 751–759.

[126] Israelachvili, J. D., D. J. Mitchell, and B. W. Ninham (1977) "Theory of Self-Assembly of Lipid Bilayers and Vesicles," *Biochimica et Biophysica Acta - Biomembranes*, **470**(2), pp. 185–201.

[127] Horvath, S. E. and G. Daum (2013) "Lipids of Mitochondria," *Progress in Lipid Research*, **52**(1), pp. 590–614.

[128] Meier, W., C. Nardin, and M. Winterhalter (2000) "Reconstitution of Channel Proteins in (polymerized) ABA Triblock Copolymer Membranes," *Angewandte Chemie International Edition*, **39**(24), pp. 4599–4602.

[129] Phillip, W. A., B. O'Neill, M. Rodwogin, M. A. Hillmyer, and E. L. Cussler (2010) "Self-Assembled Block Copolymer Thin Films as Water Filtration Membranes," *ACS Applied Materials & Interfaces*, **2**(3), pp. 847–853.

[130] Colbeau, A., J. Nachbaur, and P. M. Vignais (1971) "Enzymic Characterization and Lipid Composition of Rat Liver Subcellular Membranes," *Biochimica et Biophysica Acta - Biomembranes*, **249**(2), pp. 462–492.

[131] Spector, A. A. and M. A. Yorek (1985) "Membrane Lipid Composition and Cellular Function," *Journal of Lipid Research*, **26**(9), pp. 1015–1035.

[132] Nardin, C., J. Widmer, M. Winterhalter, and W. Meier (2001) "Amphiphilic Block Copolymer Nanocontainers as Bioreactors," *The European Physical Journal E*, **4**(4), pp. 403–410.

[133] Kita-Tokarczyk, K., K. Grumelard, T. Haefele, and W. Meier (2005) "Block Copolymer Vesicles- Using Concepts from Polymer Chemistry to Mimic Biomembranes," *Polymer*, **46**(11), pp. 3540–3563.

[134] Blanazs, A., S. P. Armes, and A. J. Ryan (2009) "Self-Assembled Block Copolymer Aggregates: From Micelles to Vesicles and Their Biological Applications," *Macromolecular Rapid Communications*, **30**(4-5), pp. 267–277.

[135] Riboldi, S. A., M. Sampaolesi, P. Neuenschwander, G. Cossu, and S. Mantero (2005) "Electrospun Degradable Polyeterurethane Membranes: Potential Scaffolds for Skeletal Muscle Tissue Engineering," *Biomaterials*, **26**(22), pp. 4606–4615.

[136] Miyahara, T., T. Hayano, S. Matsuno, M. Watanabe, and K. Miyatake (2012) "Sulfonated Polybenzophenone/poly(arene ether) Block Copolymer Membranes for Fuel Cell Applications," *ACS Applied Materials & Interfaces*, **4**(6), pp. 2881–2884.

[137] Lee, H. S., A. S. Badami, A. Roy, and J. E. McGrath (2007) "Segmented Sulfonated Poly(arylene ether sulfone)-b-polyimide Copolymers for Proton Exchange Membrane Fuel Cells. I. Copolymer Synthesis and Fundamental Properties," *Journal of Polymer Science Part A: Polymer Chemistry*, **45**(21), pp. 4879–4890.

[138] Ahmed, F., R. I. Pakunulu, G. Srinivas, A. Brannan, F. Bates, M. L. Klein, T. Minko, and D. E. Discher (2006) "Shrinkage of a Rapidly Growing Tumor by Drug-Loading Polymersomes: pH Triggered Release Through Copolymer Degradation," *Molecular Pharmaceutics*, **3**(3), pp. 340–350.

[139] Chen, L., W. Si, L. Zhang, G. Tang, Z. T. Li, and J. L. Hou (2013) "Chiral Selective Transmembrane Transport of Amino Acids Through Artificial Channels," *Journal of the American Chemical Society*, **135**(6), pp. 2152–2155.

[140] Hillmyer, M. A. and F. S. Bates (1996) "Synthesis and Characterization of Model Polyalkane- Poly(thylene Oxide) Block Copolymers," *Macromolecules*, **29**(22), pp. 6994–7002.

[141] Boinski, T., A. Cieszkowski, B. Rosa, and A. Szumna (2015) "Hybrid [n]arenes Through Thermodynamically Driven Macrocyclization Reactions," *The Journal of Organic Chemistry*, **80**(7), pp. 3488–3495.

[142] Woodle, M. C. and D. Papahadjopouos (1989) "Liposome Preparation and Size Characterization," *Methods in Enzymology*, **171**, pp. 193–217.

[143] Shen, Y., W. Song, D. R. Barden, T. Ren, C. Lang, H. Feroz, C. B. Henderson, P. Saboe, D. Tsai, H. Yan, P. J. Butler, G. C. Bazan, W. A. Phillip, R. J. Hickey, P. S. Cremer, H. Vashisth, and M. Kumar (2018) "Achieving High Permeability and Enhanced Selectivity for Angstrom-Scale Separations Using Artificial Water Channel Membranes," *Nature Communications*, **9**(1), p. 2294.

Vita

Codey Henderson

Address
Department of Chemistry
Pennsylvania State University, South Frear Room 209
University Park, PA, USA, 16802

Email
cbh153@psu.edu

Education
B.S., Chemistry
University of South Alabama
Mobile, AL
Class of 2014

Ph.D., Chemistry
Pennsylvania State University
University Park, PA
Class of 2019

Publications

Henderson, C. B., T. Yang, and P. S. Cremer (2019) "Visualization of Lipid-Conjugated Dye Aggregation in a Supported Lipid Bilayer," *In Preparation.*

Henderson, C. B., A. M. Sendecki, T. Yang, and P. S. Cremer (2019) "A Modified Free Volume Model for Supported Lipid Bilayer Diffusion," *In Preparation.*

Henderson, C. B., A. M. Sendecki, T. Yang, and P. S. Cremer (2019) "Modulation of Supported Lipid Bilayer Interactions," *In Preparation.*

Song, W., H. Joshi, R. Chowdhury, J. S. Najem, Y. Shen, C. Lang1, **C. B. Henderson**, Y. M. Tu1, Megan Farell, M. E. Pitz, C. D. Maranas, Paul S. Cremer, R. J. Hickey, S. A. Sarles, J. Hou, A. Aksimentiev, and M. Kumar (2019) "Artificial Water Channels Enable Fast and Selective Water Permeation Through Water-Wire Networks," *Nature Nanotechnology*, *Submitted.*

Shen, Y., W. Song, D. R. Barden, T. Ren, C. Lang, H. Feroz, **C. B. Henderson**, P. O. Saboe, D. Tsai, H. Yan, P. J. Butler, G. C. Bazan, W. A. Phillip, R. J. Hickey, P. S. Cremer, H. Vashisth, and M. Kumar (2018) "Achieving High Permeability and Enhanced Selectivity for Angstrom-Scale Separations Using Artificial Water Channel Membranes," *Nature Communications*, **9**(1), p.2294.